The Meteoritical Society

Meteoritics & Planetary Science 49, Nr 5, 842–871 (2014)
doi: 10.1111/maps.12285

Basaltic diversity at the Apollo 12 landing site: Inferences from petrologic examinations of the soil sample 12003

Joshua F. SNAPE[1,2,3*], Katherine H. JOY[2,4], Ian A. CRAWFORD[2,5], and Louise ALEXANDER[2,5]

[1]Department of Physical Sciences, Open University, Milton Keynes MK7 6AA, UK
[2]The Centre for Planetary Sciences at UCL-Birkbeck, Gower Street, London WC1E 6BT, UK
[3]Department of Earth Sciences, University College London, Gower Street, London WC1E 6BT, UK
[4]School of Earth, Atmospheric and Environmental Sciences, University of Manchester, Oxford Road, Manchester M13 9PL, UK
[5]Department of Earth and Planetary Sciences, Birkbeck College, University of London, Malet Street, London WC1E 7HX, UK
[*]Corresponding author. E-mail: j.snape@ucl.ac.uk

(Received 10 May 2013; revision accepted 16 February 2014)

Abstract–A detailed petrologic survey has been made of 17 basaltic chips (sized between 1 and 10 mm) from the 12003 soil sample as part of an ongoing study of basaltic diversity at the Apollo 12 landing site. An attempt has been made to classify these samples according to the well-established grouping of olivine, pigeonite, ilmenite, and feldspathic basalts. Particular attention has been paid to variations in major, minor, and trace element mineral chemistry (determined by electron microprobe analysis and laser ablation ICP-MS), which may be indicative of particular basaltic suites and less susceptible to sampling bias than bulk sample characteristics. Examples of all three main (olivine, pigeonite, and ilmenite) basaltic suites have been identified within the 12003 soil. One sample is identified as a possible new addition to the feldspathic suite, which currently consists of only one other confirmed sample. Identification of additional feldspathic basalts strengthens the argument that they represent a poorly sampled basaltic flow local to the Apollo 12 site, rather than exotic material introduced to the site by impact mixing processes. Three samples are identified as representing members of one or two previously unrecognized basaltic suites.

INTRODUCTION

The Apollo 12 mission landed on November 19th 1969 on the northwest rim of Surveyor impact crater (23.34 °W and 2.45 °S) in the eastern region of Oceanus Procellarum (Mare Cognitum). Subsequent geologic mapping by Hiesinger et al. (2000, 2003, 2010) and Morota et al. (2011) indicates that a large number of individual basaltic flows are located within the Oceanus Procellarum, including some of the youngest mare basalts (approximately 1.5 Ga) on the Moon. As discussed by Crawford et al. (2007), confirmation of the presence of such young lava flows, and information concerning their geochemistry and mineralogy, would be of great interest for our understanding of lunar magmatic evolution. None of this material has yet been identified in the existing sample collections, but given the location of the Apollo 12 landing site within the eastern region of Oceanus Procellarum, and the potential for lateral transport of material across the lunar surface by impact processes (Li and Mustard 2005), it is possible that some of this young basaltic material may be present in soils sampled by the mission. Moreover, even if exotic material derived from further west in Oceanus Procellarum is not identified in the Apollo 12 soils, a careful study of basaltic fragments within them will nevertheless provide new insights to the duration of lunar volcanism and the magmatic evolution of this region of the Moon. This is the focus of this study.

A total of 34.3 kg of samples were returned by the Apollo 12 mission (Lunar Sample Preliminary Examination Team (L.S.P.E.T.) 1970; Hiesinger and Head 2006). This included 5.9 kg of fines (material <1 cm) and chips (between 1 and 4 cm), 27.7 kg of rocks and 0.8 kg of "special" samples (including cores,

the lunar environment sample container, and the gas analysis sample container). Of the 47 rocks collected, 43 are low-Ti mare basalts (TiO_2 = 1–6 wt%; classification scheme of Neal and Taylor 1992), 3 (12010, 12034, and 12073) are regolith breccias, and 1 (12013) is a dilithologic breccia (Quick et al. 1977; Neal et al. 1994a; Korotev et al. 2011).

The most recent detailed assessment of the Apollo 12 basaltic suites was performed by Neal et al. (1994a). They established a new set of chemical criteria to discriminate among the three major basaltic suites (olivine, pigeonite, and ilmenite basalts) based on bulk Mg# (atomic Mg/[Mg+Fe]) and Rb/Sr ratios. In this scheme, olivine basalts have Mg# >46 and Rb/Sr >0.008, pigeonite basalts have Mg# <46 and Rb/Sr >0.008, and ilmenite basalts have Rb/Sr <0.008 and Mg# spanning the range of both the olivine and pigeonite suites. The feldspathic basalt 12038 falls within the ilmenite basalt classification. If one applies the Neal et al. (1994a) classification to all of the Apollo 12 basalts currently studied, the number of samples in each suite is as follows:

1. Olivine basalts—16 samples (37%)
2. Pigeonite basalts—12 samples (28%)
3. Ilmenite basalts—14 samples (33%)
4. Feldspathic basalts—1 sample (2%)

Experimental studies have determined that the olivine and pigeonite basalt mantle sources were located at a similar depth to other basaltic magmas (100–200 km; Longhi 1992a; Snyder et al. 1997). However, the ilmenite basalt source was likely located at a greater depth (350–400 km) comparable to that determined for the high-Ti picritic glasses (Longhi 1992b; Snyder et al. 1997). It remains unclear whether the feldspathic basalts represent a lava flow local to the Apollo 12 site, or if the paucity of identified samples is due to the feldspathic basalts being introduced to the site as impact ejecta (Neal et al. 1994a; Snyder et al. 1997).

Previous attempts to classify the Apollo 12 basalts have relied largely on bulk-rock characteristics (i.e., texture, modal mineralogy, and bulk compositions; James and Wright 1972; Rhodes et al. 1977; Neal et al. 1994a). Although such measurements have been made in this study, the small sizes of the samples being analyzed (1–10 mm) raises questions as to whether they are representative of the parent rocks from which they originated (Zolensky et al. 2000; Karner et al. 2003, 2004, 2006). As such, a major focus of this study has been to identify trends in major, minor, and trace element mineral chemistry, which are characteristic of individual basaltic suites. Fagan et al. (2013) have identified a relationship involving the ratio of Ti/V contents in olivine phases that appears to distinguish between ilmenite and olivine basalts. However, despite a large number of previous studies reporting major and minor element mineral chemistries of the Apollo 12 basalts (e.g., Bence et al. 1970, 1971; Grove et al. 1973; Dungan and Brown 1977), few studies have reported trace element mineral chemistries permitting such trends to be identified.

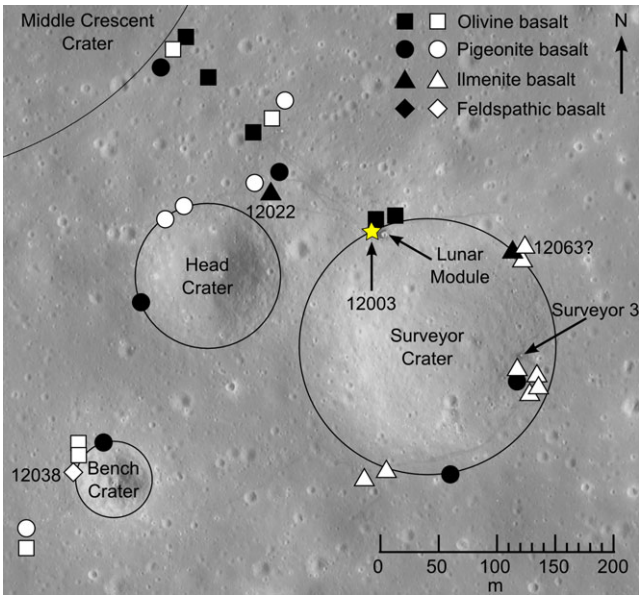

Fig. 1. Map of the Apollo 12 landing site illustrating the spatial distribution of mare basalt samples collected. Adapted from the map presented in Rhodes et al. (1977) with additional and modified symbols reflecting subsequent investigations of the Apollo 12 basalts (e.g., Neal et al. 1994a, 1994b). The sampling location of 12003 has been indicated (star symbol), as have those of the three additional samples analyzed in this study for comparative purposes (12022, 12038, and 12063). Black symbols represent more rapidly cooled vitrophyres and basalts with variolitic groundmass; white symbols represent more slowly cooled samples with ophitic and gabbroic textures. Background image is from the Lunar Reconnaissance Orbiter Narrow Angle Camera frame M175428601R (NASA/GSFC/Arizona State University).

SAMPLES AND METHODS

A total of 20 individual chips (1–10 mm) have been analyzed from the 12003 soil sample (Fig. 1). These were hand selected from the Apollo 12 sample collection at Johnson Space Center (JSC). The majority of the chips (17) have been identified as primary igneous lithologies. Six of these chips are thought to have originated from two separate parent samples at JSC but have since broken in transit to the United Kingdom. This includes the four 12003,310 chips and the two 12003,311 chips. The remaining samples include two breccias and a granulitic impactite, which will be discussed in a separate paper. In addition to the 12003 chips, three samples of well-characterized Apollo 12

Table 1. Summary of 12003 chips analyzed in this study, including the textural types assigned to them in this study, their masses, analyzed surface areas, and other comparable Apollo 12 basalts.

Sample no.	Textural type	Mass (mg)	Analyzed surface area (mm^2)	Literature comparison (similar samples)		
				Number	Apollo 12 basaltic suite	References
12003,308_1A	1	6.2	1.2	12021; 12039	Pigeonite	Weill et al. (1971); Rhodes et al. (1977)
12003,312_C	1	41.8	10.8	12052	Pigeonite	Bence et al. (1971)
12003,314_D	1	19.9	5.3	12038	Feldspathic	Beaty et al. (1979)
12003,308_2A	2	9	3.7	12002	Olivine	Grove et al. (1973); Neal et al. (1994a, 1994b)
12003,308_4A	2	8.3	2.0	12002	Olivine	Grove et al. (1973); Neal et al. (1994a, 1994b)
12003,308_8A	2	6.1	2.1	12002	Olivine	Grove et al. (1973); Neal et al. (1994a, 1994b)
12003,310_1C	2	7.6	2.6	12002	Olivine	Grove et al. (1973); Neal et al. (1994a, 1994b)
12003,310_2D	2	12.2	3.5	12002	Olivine	Grove et al. (1973); Neal et al. (1994a, 1994b)
12003,310_3A	2	7.8	3.2	12002	Olivine	Grove et al. (1973); Neal et al. (1994a, 1994b)
12003,310_4A	2	5.5	3.1	12002	Olivine	Grove et al. (1973); Neal et al. (1994a, 1994b)
12003,308_5A	3	7.5	2.6	12005	Ilmenite	Rhodes et al. (1977); Dungan and Brown (1977)
12003,308_7A	3	5.2	1.7	12005	Ilmenite	Rhodes et al. (1977); Dungan and Brown (1977)
12003,308_3A	4	6.2	1.6	12035; 12005	Olivine; Ilmenite	Reid (1971); Dungan and Brown (1977)
12003,311_1C	4	16	4.0	12016	Ilmenite	Dungan and Brown (1977)
12003,311_2C	4	5.7	1.7	12016	Ilmenite	Dungan and Brown (1977)
12003,316_C	4	13.9	4.3	12035; 12005	Olivine; Ilmenite	Reid (1971); Dungan and Brown (1977)
12003,317_D	5	16.2	5.3	12031	Pigeonite	Beaty et al. (1979)

basalts were allocated to the project by the Curation and Analysis Planning Team for Extraterrestrial Materials (CAPTEM), including two ilmenite basalts (12022,304 and 12063,330) and the feldspathic basalt (12038,263). Analyses of these have been used for comparison with the 12003 data.

As described below, each chip was split into at least two fragments. In general, the larger chip ("A-split") was used for geochemical and petrological analysis, and a smaller second ("B-split") chip was retained for future radiometric age dating. If more than two fragments resulted from the splitting process, these were referred to as "C-" and "D-splits." For the smallest (<2 mm) samples, a New Wave 213 nm laser with a beam width of 25 μm was used to begin the cutting process to reduce the overall mass loss. Where necessary, the samples were then split with a fine scalpel blade. For samples much larger than 2 mm, this method was impractical due to limitations of the laser system and splitting was performed entirely with either a scalpel or a pair of surgical bone cutters.

The samples to be used for petrologic analyses (Table 1) were mounted in EPOTEK epoxy resin blocks. Any surficial resin was ground away with silicon carbide paper to expose the samples. The exposed sample surfaces were then polished with either aluminum oxide or diamond paste on pellon cloths using an alcohol-based lubricant. Finally, the samples were coated with carbon to facilitate electron microprobe analysis (EMPA).

Energy dispersive spectroscopy (EDS) analysis of the samples was performed using a JEOL JXA-8100 electron microprobe analyzer at UCL/Birkbeck with an accompanying Oxford Instruments EDS probe and INCA software package. The probe was operated at a 15 kV accelerating voltage, with a 10 nA beam current and 1 μm diameter beam. This included the acquisition of backscattered electron (BSE) images, elemental mapping and bulk sample, and area compositions. Element maps of the samples were "colorized" and combined using the GNU Image Manipulation Program (GIMP) to generate false color element maps (see Appendix S3) following similar methods previously used by Joy et al. (2008, 2011) and Snape et al. (2011a, 2011b).

Modal mineralogies (Table 2) were obtained from the BSE images and X-ray element maps using GIMP. A majority of the individual phases within each sample were automatically identified based on their grayscale tone in the BSE images. This technique was effective in many cases where the tonal differences between the phases were clear. However, for phases with very similar grayscale tones in the BSE images (for example, pyroxene and olivine), or in the case of very compositionally zoned phases, it was often necessary to use the elemental maps to refine the selection. Having identified the phases within a given sample or area, it was then possible to use GIMP to count the pixels associated with each phase and calculate the modal mineralogies from these pixel

Table 2. Modal mineralogies (% of analyzed area) of the 12003 chips. Also included are values obtained from the fine-grained 12003,312 groundmass (i.e., excluding mafic phenocrysts).

	Pyroxene	HCP	LCP	Olivine	Plagioclase	Silica	Ilmenite	Spinel	Sulfide	FeNi metal	Phosphates	Glass/mesostasis
12003,308_1A	51	–	–	–	39	6	4	<1	<1	–	–	<1
12003,308_2A	52	–	–	17	27	1	3	1	<1	<1	<1	<1
12003,308_3A	–	3	31	37	26	–	1	2	<1	<1	–	<1
12003,308_4A	60	–	–	19	18	<1	1	1	<1	<1	<1	<1
12003,308_5A	–	13	72	10	1	–	2	3	–	–	–	–
12003,308_7A	–	33	49	11	5	–	<1	2	<1	–	<1	<1
12003,308_8A	56	–	–	18	24	<1	1	0	–	–	<1	<1
12003,310_1C	47	–	–	17	31	1	4	1	<1	<1	<1	<1
12003,310_2D	49	–	–	26	21	<1	1	2	<1	<1	<1	<1
12003,310_3A	60	–	–	4	32	1	2	<1	<1	–	<1	<1
12003,310_4A	49	–	–	22	23	<1	2	2	<1	–	<1	<1
12003,311_1C	42	–	–	19	36	<1	2	2	<1	<1	<1	<1
12003,311_2C	43	–	–	18	38	<1	<1	1	<1	<1	<1	<1
12003,312_C	73	–	–	1	21	2	2	<1	–	<1	–	–
12003,312_C (groundmass)	45	–	–	–	50	2	4	<1	–	–	–	–
12003,314_D	39	–	–	–	55	4	1	1	<1	<1	<1	<1
12003,316_C	–	2	15	44	37	–	<1	1	<1	<1	<1	<1
12003,317_D	57	–	–	–	34	5	4	<1	<1	<1	<1	<1

HCP = high-Ca pyroxene, LCP = low-Ca pyroxene. Repeat analyses of the same BSE images and element maps indicate that absolute uncertainties on these modal abundances are between 0 and 5%.

counts. The accuracy and reproducibility of this method was previously demonstrated with several well-characterized Apollo 12 basalts (Snape et al. 2011a, 2011b; Snape 2012).

Major and Minor Element Bulk Compositions

The bulk sample compositions (Table 3) were measured using the EDS probe and INCA software package by performing multiple raster beam analyses (RBA) across the sample areas with acquisition times of 480 s (see also Joy et al. 2010, 2011; Snape et al. 2011a, 2011b). Prior to each set of measurements, the EDS detector was calibrated by analyzing a Co standard. Repeat RBA were averaged together and the mean result was normalized to reduce the effects of void spaces, mineral edge effects, and small fractures. The errors quoted for these average values are the 1σ standard deviations between the individual RBA, and therefore indicate the instrumental precision of the measurements. Samples that were too large to fit within the maximum field of view of the electron microprobe were divided into multiple areas within which the area scans were performed. The sizes of these areas were then measured using the image processing program ImageJ (Rasband 1997–2013; Schneider et al. 2012) and used to weight each set of area scan results (based on their relative sizes) prior to combining them to obtain an overall sample composition.

To monitor and assess the accuracy and precision of the EDS system, measurements were obtained from a section of the U.S. Geological Survey (USGS) BCR-2 basaltic glass standard before and after each set of sample analyses. Comparison of these measurements with the composition reported by the USGS (http://crustal.usgs.gov/geochemical_reference_standards/; Wilson 1997) indicates a relative error of <6% for almost all elements present at concentrations >0.1 wt% (including Na, Mg, Al, Si, K, Ca, Ti, Cr, Mn, and Fe). An exception to this is P, for which accurate measurements at low concentrations are difficult to obtain by EDS due to an overlap between the P Kα and Si Kα X-ray emission lines.

Differences in density between individual phases within the area being analyzed are known to result in a potentially significant error associated with RBA and similar defocused or broad beam analyses (Dowty et al. 1973; Albee et al. 1977). This invariably leads to underestimations for concentrations of heavier elements such as Mg and Fe, and overestimations of lighter elements such as Al (Dowty et al. 1973). As such, a correction outlined by Warren (1997) has been used to correct the analyses made in this investigation. A more detailed discussion of the implementation of Warren's (1997) method used in this study can be found in Snape (2012).

Major and Minor Element Mineral Chemistry

Major and minor element analyses of individual mineral phases were performed with the JEOL JXA-8100 electron microprobe wavelength dispersive spectroscopy (WDS) system at UCL/Birkbeck. Measurements were made using a 15 kV accelerating voltage, a 25 nA beam current, and a 1 μm diameter beam. A peak acquisition time of 20 s (with a background acquisition time of 10 s) was used for a majority of the elements analyzed; a peak time of 10 s and a background time of 5 s were used for Na. All measurements were calibrated with well-characterized standard samples, including: jadeite (Na), orthoclase (K), olivine (Mg, Fe), apatite (P, Ca) corundum (Al), wollastonite (Si), rutile (Ti), Cr-metal (Cr), Mn-metal (Mn), Ni-metal (Ni) V-metal (V), and Co-metal (Co).

Measurements with analytical totals (in oxide weight percent) of <97.5% or greater than 102.5% were rejected. The remaining measurements were then subjected to stoichiometric checks to confirm that the compositions agreed with canonically accepted mineral formulae (Deer et al. 1966; Papike et al. 1991). Additional corrections were applied for Fe/Co and Ti/V Kα-peak and Kβ-peak overlaps, based on repeat measurements of pure metal standards. As with the EDS RBA, the USGS BCR-2 basaltic glass standard was used as an external standard to allow the accuracy and precision of the data to be assessed. Multiple measurements of the BCR-2 standard were obtained throughout the course of each set of analyses. A majority (88%) of these measurements are within the errors quoted by the USGS for the standard glass for elements present at concentrations >0.1 wt%. The relative errors between the measured concentrations and the USGS values are also consistently below 5% for a majority of these elements. An exception to this is Na (typically below 10%) for which accurate measurements are difficult to obtain due to the element's volatility upon interaction with the electron beam.

Trace Element Mineral Chemistry

Mineral trace element chemistries were determined using a laser ablation inductively coupled plasma mass spectrometer (LA-ICP-MS), with a similar analytical procedure as described by Joy et al. (2010, 2011). The instrumental setup consisted of a New Wave Research UP-213 aperture imaged frequency quintupled laser ablation system (213 nm) coupled to an Agilent 750a quadrupole-based ICP-MS with a shield torch to reduce

Table 3. Normalized major and minor element bulk chemistries of the 12003 chips, reported as oxide wt% values. Also included are values obtained from the fine-grained 12003,312 groundmass (i.e., excluding mafic phenocrysts).

	12003,308_1A	12003,308_2A	12003,308_3A	12003,308_4A	12003,308_5A	12003,308_7A	12003,308_8A	12003,310_1C	12003,310_2D
SiO_2	45.80 ± 0.25	44.48 ± 0.09	42.44 ± 0.08	45.54 ± 0.14	47.82 ± 0.07	48.47 ± 0.06	46.22 ± 0.16	42.79 ± 0.11	42.67 ± 0.10
TiO_2	4.77 ± 0.06	2.58 ± 0.07	1.22 ± 0.02	2.13 ± 0.04	2.43 ± 0.06	1.23 ± 0.02	1.62 ± 0.04	3.75 ± 0.04	2.16 ± 0.02
Al_2O_3	12.86 ± 0.04	10.12 ± 0.07	9.47 ± 0.14	7.19 ± 0.07	2.16 ± 0.03	3.79 ± 0.03	9.00 ± 0.07	9.50 ± 0.04	7.40 ± 0.05
FeO	19.85 ± 0.11	20.23 ± 0.13	21.73 ± 0.14	19.83 ± 0.14	18.48 ± 0.06	16.24 ± 0.08	17.89 ± 0.06	21.14 ± 0.08	22.20 ± 0.13
MnO	0.26 ± 0.04	0.29 ± 0.03	0.27 ± 0.02	0.30 ± 0.02	0.32 ± 0.02	0.28 ± 0.03	0.26 ± 0.03	0.26 ± 0.01	0.29 ± 0.03
MgO	4.34 ± 0.11	11.84 ± 0.08	17.03 ± 0.11	16.13 ± 0.09	20.91 ± 0.04	19.41 ± 0.04	15.64 ± 0.06	11.58 ± 0.05	15.58 ± 0.09
CaO	11.12 ± 0.13	9.13 ± 0.03	6.54 ± 0.06	7.68 ± 0.07	6.09 ± 0.03	8.75 ± 0.04	8.31 ± 0.04	8.53 ± 0.04	7.25 ± 0.03
Na_2O	0.40 ± 0.02	0.38 ± 0.01	0.37 ± 0.01	0.30 ± 0.01	0.23 ± 0.02	0.23 ± 0.01	0.35 ± 0.01	1.28 ± 0.03	0.72 ± 0.03
K_2O	0.09 ± 0.01	0.06 ± 0.01	0.03 ± 0.01	0.03 ± 0.01	0.00 ± 0.01	0.01 ± 0.01	0.03 ± 0.01	0.07 ± 0.01	0.05 ± 0.01
Cr_2O_3	0.23 ± 0.02	0.71 ± 0.03	0.79 ± 0.03	0.72 ± 0.03	1.51 ± 0.03	1.53 ± 0.03	0.58 ± 0.03	0.65 ± 0.03	1.37 ± 0.03
P_2O_5	0.27 ± 0.02	0.17 ± 0.03	0.10 ± 0.02	0.13 ± 0.02	0.04 ± 0.02	0.05 ± 0.02	0.11 ± 0.02	0.46 ± 0.02	0.31 ± 0.01
Mg#	28.07	51.08	58.30	59.20	66.87	68.07	60.93	49.42	55.60
No. of raster beam analyses	5	10	10	20	10	10	10	10	10

	12003,310_3A	12003,310_4A	12003,311_1C	12003,311_2C	12003,312_C	12003,312_C (groundmass)	12003,314_D	12003,316_C	12003,317_D
SiO_2	46.16 ± 0.07	42.63 ± 0.09	43.07 ± 0.07	45.09 ± 0.27	45.88 ± 0.09	44.91 ± 0.08	47.29 ± 0.24	40.54 ± 0.09	45.28 ± 0.15
TiO_2	2.72 ± 0.02	2.74 ± 0.03	2.48 ± 0.04	0.98 ± 0.04	3.43 ± 0.03	4.67 ± 0.05	1.98 ± 0.06	0.91 ± 0.02	3.91 ± 0.11
Al_2O_3	11.03 ± 0.05	7.58 ± 0.05	11.52 ± 0.03	12.19 ± 0.05	10.05 ± 0.04	13.10 ± 0.02	16.71 ± 0.07	11.67 ± 0.06	11.10 ± 0.09
FeO	18.62 ± 0.06	22.16 ± 0.07	19.27 ± 0.08	17.83 ± 0.17	19.99 ± 0.09	22.94 ± 0.14	14.56 ± 0.23	20.50 ± 0.09	19.68 ± 0.15
MnO	0.28 ± 0.02	0.30 ± 0.03	0.26 ± 0.03	0.25 ± 0.03	0.27 ± 0.02	0.28 ± 0.03	0.18 ± 0.02	0.25 ± 0.02	0.27 ± 0.03
MgO	8.88 ± 0.03	14.90 ± 0.07	12.81 ± 0.04	12.75 ± 0.12	7.79 ± 0.04	2.52 ± 0.01	4.71 ± 0.06	17.32 ± 0.07	5.51 ± 0.04
CaO	10.77 ± 0.02	7.48 ± 0.05	9.10 ± 0.03	9.40 ± 0.04	10.47 ± 0.03	10.30 ± 0.04	12.66 ± 0.04	6.73 ± 0.05	11.29 ± 0.05
Na_2O	0.65 ± 0.01	0.48 ± 0.02	0.52 ± 0.01	0.80 ± 0.01	1.08 ± 0.02	0.77 ± 0.01	1.16 ± 0.02	1.11 ± 0.02	2.06 ± 0.02
K_2O	0.08 ± 0.01	0.05 ± 0.01	0.02 ± 0.01	0.05 ± 0.01	0.07 ± 0.01	0.11 ± 0.01	0.06 ± 0.01	0.03 ± 0.01	0.08 ± 0.01
Cr_2O_3	0.50 ± 0.02	1.43 ± 0.04	0.67 ± 0.01	0.30 ± 0.02	0.58 ± 0.02	0.04 ± 0.04	0.26 ± 0.03	0.60 ± 0.02	0.26 ± 0.03
P_2O_5	0.31 ± 0.03	0.25 ± 0.03	0.27 ± 0.02	0.36 ± 0.02	0.39 ± 0.02	0.37 ± 0.02	0.43 ± 0.02	0.35 ± 0.03	0.55 ± 0.02
Mg#	45.98	54.54	54.26	56.06	41.00	16.37	36.62	60.12	33.33
No. of raster beam analyses	10	10	10	10	25	5	10	10	15

Errors are 1σ standard deviations of the specified number of raster beam analyses.

polyatomic interferences. The laser source was operated with a pulse frequency of 10 Hz and a fluence of 3–4 mJ cm^{-2}. Instrumental background levels were established by analyzing the mixed He gas and Ar carrier gas with the laser off for 30 s. The sample was then ablated for 30 s with a 55 μm spot size.

Data were reduced using the GEMOC GLITTER© software program (Van Achterberg et al. 2001; Macquarie Ltd. 2005—http://www.glitter-gemoc.com/). Plagioclase and pyroxene analyses were calibrated with CaO (wt%) concentrations obtained from WDS EMPA as internal standard values and the NIST SRM 612 glass as an external standard (Pearce et al. 1997). Olivine analyses were calibrated with MnO (wt%), using the NIST SRM 610 glass as an external standard. Repeat measurements of the NIST glasses were compared with the preferred average NIST 610 and 612 element concentrations reported by Pearce et al. (1997) to assess their accuracy. The difference between the values in this study and the Pearce et al. (1997) values was <10% for all elements analyzed, and typically <5%. The relative standard deviation of all the NIST 610 standard repeat measurements had a total range of between 1 and 15% (1σ) for all elements analyzed except Au and Cu (between 1 and 22%). The relative standard deviation of all the NIST 612 standard repeat measurements was less than 15% (1σ) for a majority of the elements analyzed. However, several elements (e.g., Zn, Au, and U) appear to be less reproducible, with relative standard deviations of between 3 and 28%.

RESULTS

Bulk Compositions

Major and minor element bulk compositions for the 12003 samples are listed in Table 3. A majority of the samples have between 1.2 and 4.8 wt% TiO_2, consistent with low-Ti mare basalts (Neal and Taylor 1992). The two exceptions to this are 12003,311_2C and 12003,316_C (0.98 and 0.91 wt% TiO_2, respectively). The Al content for the majority of the samples varies between 7.2 and 12.9 wt% Al_2O_3. Significant outliers from this range include 12003,308_5A and 12003,308_7A (2.2 and 3.8 wt%, respectively), and 12003,314_D (16.7 wt%). The bulk Mg# vary between 28 and 68, with the highest values occurring in the samples 12003,308_5A (Mg# = 67) and 12003,308_7A (Mg# = 68), and the lowest in 12003,308_1A.

Petrography

Initial observations by both optical and electron microscopy revealed textural differences between the samples. The variety of modal mineralogies and major and minor element bulk compositions of the samples are also broadly consistent with these observations. For this discussion, a preliminary petrographic grouping has been defined based on the textural similarities between the samples, their modal mineralogies, and bulk compositions (Tables 2 and 3).

Type 1

Three of the 12003 samples have groundmass textures that vary from subophitic to variolitic. The finest grained (approximately 0.01–0.40 mm) of these samples (12003,308_1A) has a porphyritic texture with phenocrysts of pyroxene and a subophitic groundmass of prominently zoned pyroxene (51% by modal abundance) and laths of plagioclase (39%; approximately 400 × 50 μm; Fig. 2a). Elongated crystals of plagioclase (approximately 400 × 50 μm) are common throughout the sample. A general alignment of many of these laths is also observed, although this is not consistent in all cases. Many of the laths have an intrafasciculate texture with hollow cores containing pyroxene. Other plagioclase grains occur adjacent to pyroxene grains forming a variolitic texture. 12003,308_1A also stands out as having significantly more crystalline silica than any of the other 12003 samples (6%; Table 2). This occurs as anhedral grains (approximately 10–75 μm) of an undetermined silica polymorph. These are commonly adjacent to the most Fe-rich areas of pyroxene grains. The next most abundant minor mineral in this sample is ilmenite (4%). This also forms elongated laths (approximately 150 × 10 μm) that sometimes cross-cut, and in other instances are cross-cut by, the larger plagioclase grains. Accessory minerals are common around the more evolved pyroxene rims and silica grains. These include small (<10 μm) grains of troilite, FeNi metal, and apatite.

12003,312_C has a porphyritic texture with large (up to approximately 1.6 mm) mafic phenocrysts in a fine-grained (approximately 5–80 μm) variolitic matrix (Fig. 2b). The matrix is composed of thin plagioclase laths (approximately 60 × 5 μm, 50% by mode; Table 2); interstitial pyroxene grains (approximately 50 × 10 μm); small ilmenite needles (approximately 15 × 2 μm, 4% by mode); and occasional interstitial grains of a silica polymorph (approximately 10–30 μm; 2%). A majority of the phenocrysts are elongated (approximately 0.3–1.6 mm) zoned pyroxene. The sample also contains several olivine phenocrysts, including two skeletal olivine grains (approximately 0.2–0.5 mm; Fig. 2b). Subhedral to euhedral spinel crystals (30–90 μm) are also present throughout the sample. These occur as isolated grains in the fine-grained matrix

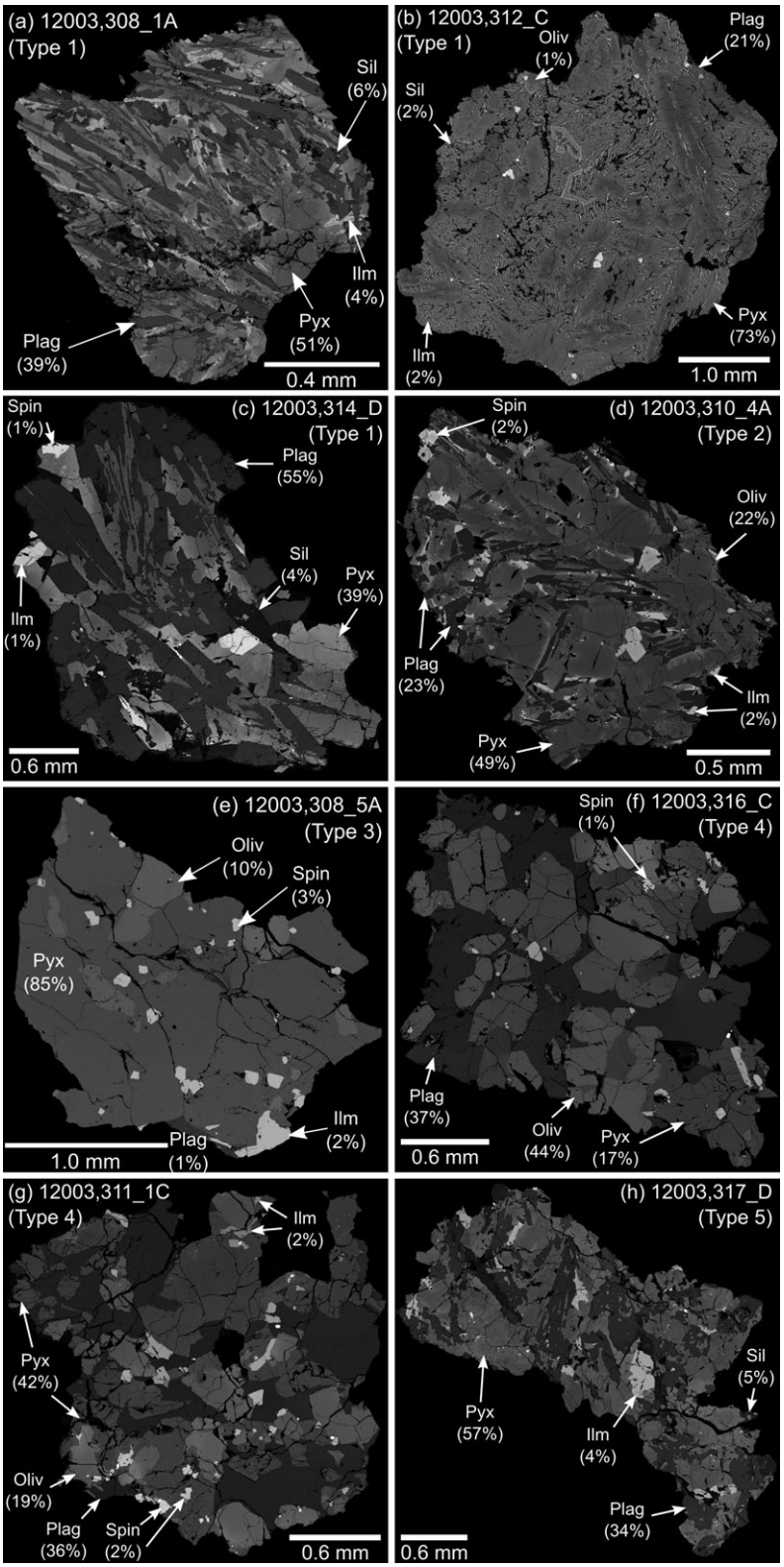

Fig. 2. Backscattered electron (BSE) images of examples of the (a–c) type 1, (d) type 2, (e) type 3, (f–g) type 4, and (h) type 5, 12003 chips. Major and minor phases have been indicated along with their modal abundances. Other sample images and element maps are provided in Appendix S3. Pyx = pyroxene; Plag = plagioclase; Oliv = olivine; Sil = silica; Ilm = ilmenite; Spin = spinel.

as well as adjacent to and partially enclosed in the larger pyroxene and olivine phenocrysts. The sample contains a single glomerophyric spinel cluster that appears to be associated with a small (30 μm) grain of FeNi metal. Several other smaller (10–20 μm) independent FeNi metal grains are present in the 12003,312_C groundmass.

12003,314_D is a more coarse-grained (0.2–1.1 mm; Fig. 2c) subophitic sample composed mostly of plagioclase (55% by mode) and pyroxene (39%). The sample has a higher abundance of plagioclase, and consequently is more Al-rich, than any of the other 12003 samples (Al_2O_3 = 16.7 ± 0.1 wt%; Table 3). The minor phases in 12003,314_D include silica, spinel, and ilmenite (Table 2). These form intergrowths with plagioclase and pyroxene on a smaller scale (<50 μm) than that of the two major phases. Large (0.1–0.6 mm) crystals of a silica polymorph are common throughout the sample (4% by modal abundance). These are often fractured and embayed. Spinel is the next most abundant phase in 12003,314_D (1%) and forms subhedral ulvöspinel crystals (approximately 0.1–0.3 mm; Fig. 2c). The largest of these also contains small (approximately 10–30 μm) exsolved grains of ilmenite. Ilmenite is also present (1% by modal abundance) as separate subhedral crystals (approximately 0.03–0.30 mm; Fig. 2c). The sample contains several regions of mesostasis containing pyroxferroite, K-feldspar, high-K glass, phosphate, troilite, and Fe metal grains. The Fe metal in 12003,314_D occurs as small (approximately 5 μm) exsolved grains in the troilite phases.

Type 2

Seven samples contain olivine phenocrysts (4–26% by modal abundance) and have more ophitic groundmass textures than the type 1 samples composed of pyroxene (47–60%) and plagioclase (18–32%; Fig. 2d). The plagioclase grains in these samples are less elongate and more tabular than those in 12003,308_1A (approximately 350 × 100 μm). However, the plagioclase grains in several of the samples have similar intrafasciculate textures and radiating plagioclase-pyroxene. These samples contain more spinel than 12003,308_1A, but less ilmenite (1–4% by modal abundance) and less silica (≤1%). The spinel crystals occur as subhedral to euhedral microphenocrysts between approximately 10–180 μm in size. The majority of the spinels are adjacent to and only partially enclosed by olivine. However, several small (approximately 10–30 μm) grains are completely enclosed within the larger olivine phenocrysts (Fig. 2d). The spinel grains are commonly grouped together to form glomerophyric clusters. Ilmenite is present as both anhedral interstitial grains and subhedral laths. Accessory minerals such as FeNi metal, troilite, apatite, and high-K glass are present throughout these samples. These are most common in the Fe-rich pyroxene rims, and often occur adjacent to silica grains and within fine-grained (<10 μm) mesostasis areas.

Type 3

Two samples (12003,308_5A and 12003,308_7A) have coarser grained (approximately 0.25–0.80 mm) textures. They are almost entirely composed of mafic minerals (93–95% by modal abundance) and contain little plagioclase (1–5%), resulting in higher bulk-rock Mg# (67–68) than any of the other 12003 samples (Mg# = atomic Mg/[Fe+Mg] × 100; Fig. 2e). Pyroxene is the most abundant phase in these samples (82–85%). Olivine (10–11%) occurs as rounded medium-large (approximately 65–550 μm) grains entirely enclosed by the pyroxene phases of these samples. Subhedral to euhedral spinel grains (approximately 30–100 μm) are also relatively common (2–3%). Exsolved ilmenite, small (<10 μm) troilite grains, and associated FeNi metal grains were identified within one of the more Ti-rich spinel in 12003,308_5A. Separate similarly sized merrillite and FeNi metal grains were also identified in both samples. No silica was identified in either of these samples.

Type 4

12003,308_3A and 12003,316_C also have coarser grained (approximately 0.1–0.8 mm) textures, composed of mostly subhedral to euhedral crystals of olivine (37–44%) and anhedral pyroxene (17–34%) poikilitically enclosed by plagioclase (26–37%; Fig. 2f). Spinel is present as a minor phase (1–2% by modal abundance), forming subhedral microphenocrysts that range between approximately 20–100 μm in size and occasionally exhibit patches of ilmenite exsolution approximately 5–15 μm in size. The samples also contain separate subhedral to anhedral ilmenite grains (30–130 μm; <1%). Accessory minerals include grains of troilite and associated FeNi metal blebs (<10 μm). Several small (<10 μm) grains of K-feldspar were also identified in 12003,308_3A, most notably in a region of mesostasis adjacent to an olivine grain. No silica was identified in either of these samples.

The two samples from the 12003,311 parent (12003,311_1C; 12003,311_2C) have textures similar to the 12003,308_3A and 12003,316_C samples (Fig. 2g). However, these samples contain more pyroxene (42–43%) and less olivine (18–19%). Several of the olivine grains appear to exhibit pyroxene overgrowths. The pyroxene in the 12003,311 samples exhibits patchy zoning and several grains contain 1–10 μm thick

Table 4. Inventory of the range of major and minor element mineral chemistries identified in the pyroxene, plagioclase, olivine, spinel, and ilmenite phases of the 12003 chips.

		Pyroxene			Plagioclase		Olivine	Spinel			Ilmenite
Sample no.	Textural type	Wo	En	Fs	An	Or	Fo	2Ti	Al	Cr	MgO (wt%)
12003,308_1A	Type 1	10–38 14–38[a]	0.4–46 8.1–56[a]	31–85 22–62[a]	85–93	0.2–1.4	–	74–89	4.7–7.3	5.7–19	0.0–0.1
12003,312_C	Type 1	9.4–28 7.9–39[a]	2.7–30 30–64[a]	55–76 22–41[a]	85–91	0.4–0.7	41–64	13–81	6.0–26	11–63	–
12003,314_D	Type 1	12–32	4.0–53	30–83	87–93	0.1–1.3	–	89–92	3.7–4.7	4.1–7.2	0.1–0.3
12003,308_2A	Type 2	9.7–40	1.0–57	20–83	82–92	0.2–5.5	3.3–73	11–83	5.6–25	11–63	0.1–1.7
12003,308_4A	Type 2	7.5–39	4.9–63	17–83	88–93	0.3–0.9	45–71	10–82	5.9–28	12–64	1.0–3.4
12003,308_8A	Type 2	6.4–38	2.8–66	18–85	85–94	0.2–5.2	47–74	11–85	7.7–27	11–64	0.1–0.3
12003,310_1C	Type 2	8.6–40	2.0–60	18–80	88–93	0.2–2.0	44–73	10–73	7.3–25	20–66	0.1–0.4
12003,310_2D	Type 2	8.3–36	7.7–61	20–76	88–92	0.2–2.1	41–72	10–86	5.7–29	8.3–65	0.6–1.7
12003,310_3A	Type 2	9.5–33	1.1–59	22–86	87–92	0.2–0.9	48–71	10–62	12–26	26–66	0.1–0.2
12003,310_4A	Type 2	11–35	9.7–58	21–70	88–91	0.2–0.4	39–73	9.6–79	6.5–25	14–66	0.1–1.7
12003,308_5A	Type 3	(HCP) 27–41 (LCP) 7.2–17	41–53 56–66	15–23 25–31	90	0.7–0.8	62–68	21–63	11–31	26–52	5.2–5.7
12003,308_7A	Type 3	(HCP) 29–38 (LCP) 4.2–20	45–51 55–66	16–20 25–31	77–93	0.1–5.1	61–68	19–48	23–32	38–55	–
12003,308_3A	Type 4	(HCP) 29–38 (LCP) 3.7–22	43–49 51–62	19–23 25–38	86–93	0.2–1.1	55–73	51–65	10–15	25–35	4.4–4.5
12003,316_C	Type 4	(HCP) 32–33 (LCP) 9.1–19	47–47 55–61	20–21 24–30	85–90	0.1–0.9	61–66	23–65	11–26	24–51	5.4–6.4
12003,311_1C	Type 4	8.7–39	22–62	17–64	88–90	0.1–0.3	42–63	36–80	6.5–23	13–41	1.7–3.2
12003,311_2C	Type 4	24	39	37	91	0.2	61	–	–	–	–
12003,317_D	Type 5	8.5–34	10–44	30–79	77–94	0.1–1.6	–	–	–	–	0.5–0.9

[a]Pyroxene phenocrysts.

Aug = augite, Pig = pigeonite, HCP = high-Ca pyroxene, LCP = low-Ca pyroxene. Pyroxene values marked with an asterisk were obtained from phenocryst phases in 12003,308_1A and 12003,312_C. Wo = atomic Ca/[Mg+Fe+Ca] × 100; En = atomic Mg/[Mg+Fe+Ca] × 100; Fs = atomic Fe/[Mg+Fe+Ca] × 100; An = atomic Ca/[Ca+Na+K] × 100; Or = atomic K/[Ca+Na+K] × 100; Fo = atomic Mg/[Fe+Mg] × 100; 2Ti = atomic 2 × Ti/[2 × Ti+Al+Cr] × 100; Al = atomic Al/[2 × Ti+Al+Cr] × 100; Cr = atomic Cr/[2 × Ti+Al+Cr] × 100.

lamellae. These have two orientations, which intersect at approximately 40°, and are occasionally slightly curved. The 12003,311 samples also include an unidentified phosphate species as an accessory phase, in addition to anhedral grains of FeNi metal, sulfide, and K-feldspar (approximately 5–20 μm). Silica is rare (<0.1% by modal abundance) in both samples, but occurs adjacent to plagioclase, ilmenite, and the FeNi metal grains.

Type 5

12003,317_D has a more granular texture than the other 12003 samples and is composed mostly of pyroxene (57% by mode) and plagioclase (34%; Fig. 2h). The plagioclase occasionally occurs as elongated subhedral grains with intrafasciculate textures, but more commonly as anhedral grains with irregular resorbed edges. The pyroxene in 12003,317_D encloses plagioclase and exhibits irregular patchy zoning. The most abundant minor phase in 12003,317_D is a silica polymorph (5% by mode; Table 2). This is present as approximately 70–600 μm grains, which tend to be adjacent to and intergrown with the plagioclase phases. Several smaller grains are completely enclosed in plagioclase (Fig. 2h). Anhedral ilmenite grains are also common (4%) and typically occur at the boundaries between the plagioclase and pyroxene phases. Mesostasis areas are located toward the edges of pyroxene phases and adjacent to silica grains. These contain pyroxferroite, high-K glass, and phosphate phases (5–50 μm in size). The pyroxenes also contain exsolved Fe metal grains (5–20 μm).

Mineral Chemistry

Plagioclase

For a majority of the 12003 samples, plagioclase are $An_{85–95}$ (An = atomic Ca/[Ca+Na+K] × 100; Table 4; Fig. 3a). Exceptions to this are 12003,308_7A, ($An_{77–93}$) and 12003,317_D ($An_{77–94}$). Abundances of K_2O in the 12003 plagioclase crystals are typically low for lunar materials, with most samples here having compositions of $Or_{0.1–2.1}$ (Or = atomic K/[Ca+Na+K] × 100; Table 4). However, three samples (12003,308_2A; 12003,308_7A; 12003,308_8A) have slightly more Na-rich compositions

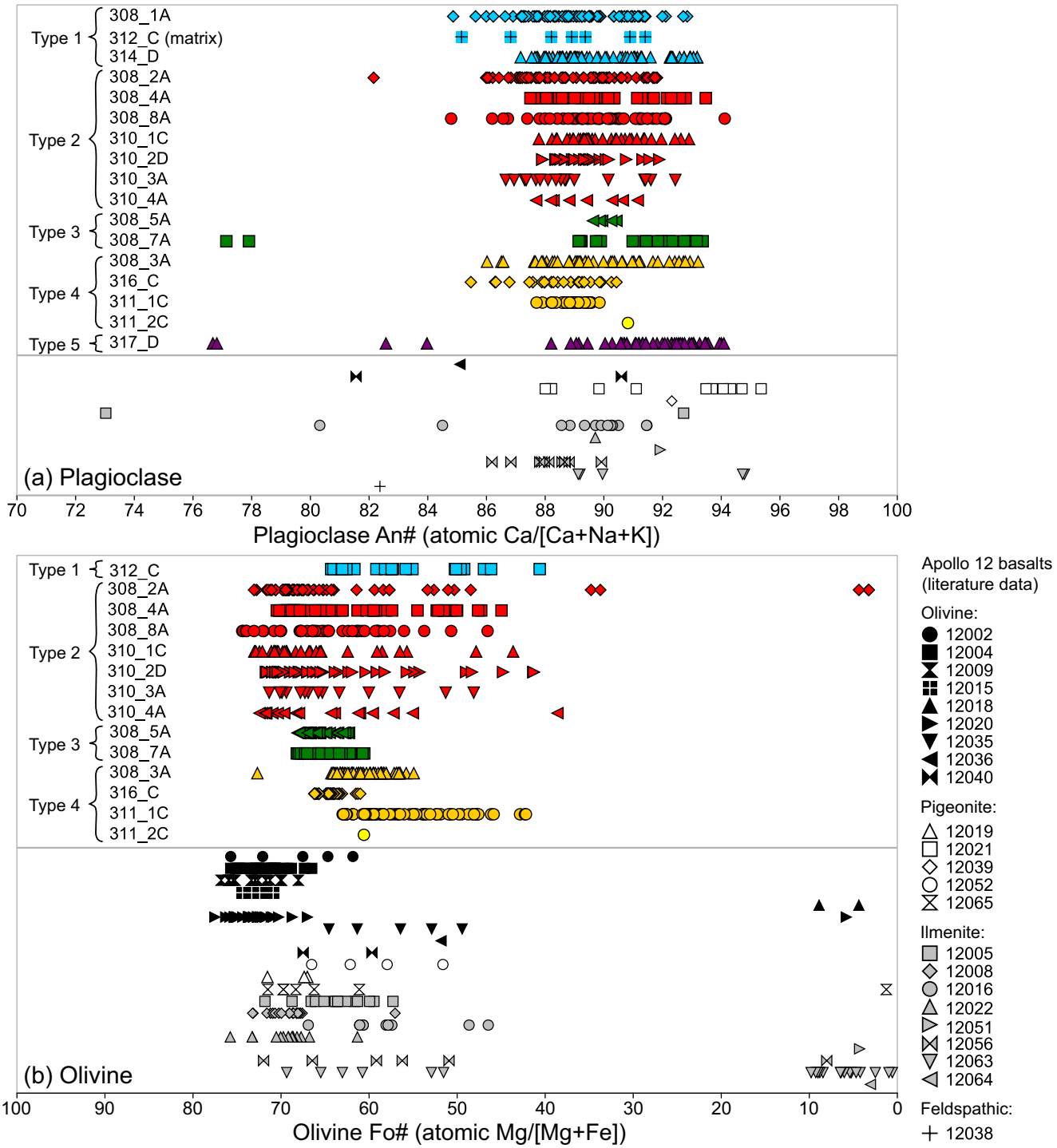

Fig. 3. Ranges of (a) plagioclase anorthite content (An: atomic Ca/[Ca+Na+K] × 100) and (b) olivine forsterite content (Fo: atomic Mg/[Mg+Fe] × 100) within the 12003 chips. The 12003 plagioclase and olivine compositions are compared with those within other Apollo 12 samples (Bence et al. 1970; Anderson and Smith 1971; Brett et al. 1971; Brown et al. 1971; El Goresy et al. 1971; Hollister et al. 1971; Keil et al. 1971; Kushiro et al. 1971; Newton et al. 1971; Taylor et al. 1971; Weill et al. 1971; Butler 1972; Crawford 1973; Dungan and Brown 1977; Marvin and Walker 1985).

up to $Or_{5.5}$. The discrepancy in plagioclase compositions between the type 3 samples is interpreted as a result of undersampling of plagioclase in 12003,308_5A. The 12003 plagioclase rare earth element (REE) compositions typically have La_{cn}/Lu_{cn} ratios of between 1.5 and 3.8 and positive Eu-anomalies (typical range of Eu/

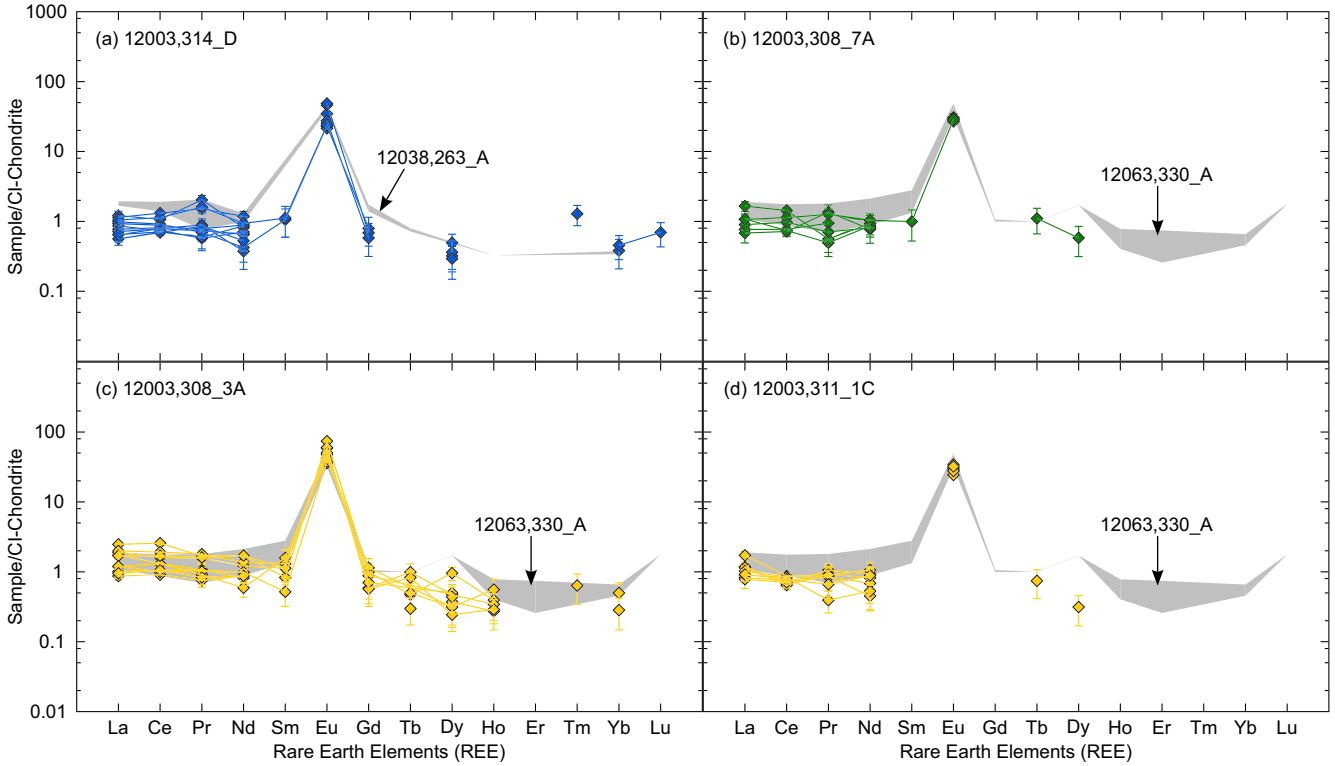

Fig. 4. Chondrite normalized (Anders and Grevesse 1989) REE patterns for plagioclase within 12003,314_D; 12003,308_7A; 12003,308_3A; and 12003,311_1C. Error bars represent 1σ errors. 12003 data have been compared with those obtained from the ilmenite basalt 12063,330 and the feldspathic basalt 12038,263.

Eu* = 10–58; where Eu/Eu* = $Eu_{cn}/\sqrt{[Sm_{cn} \times Gd_{cn}]}$ and cn indicates values normalized to CI concentrations reported by Anders and Grevesse 1989) (Fig. 4). The trivalent plagioclase REE concentrations in the 12003 samples vary between 0.2 and 8.2 × CI abundances.

Pyroxene

Most of the 12003 samples contain pyroxene grains that exhibit prominent compositional zoning between magnesian cores and more Fe-rich rims (Figs. 5, 6, and 7; Table 4). This core-rim trend is less clear in the samples with more patchy pyroxene zonation (12003,311_1C; 12003,311_2C; 12003,317_D) and the subophitic-intergranular sample 12003,314_D. The porphyritic samples 12003,308_1A and 12003,312_C contain two populations of pyroxene phases: more magnesian phenocrysts (12003,308_1A: $Wo_{14–38}En_{8.1–56}Fs_{22–62}$; 12003,312_C: $Wo_{7.9–39}En_{30–64}Fs_{22–41}$; Wo = atomic Ca/[Fe+Mg+Ca] × 100; En = atomic Mg/[Fe+Mg+Ca] × 100; Fs = atomic Fe/[Fe+Mg+Ca] × 100), and comparatively Fe-rich groundmass pyroxene (12003,308_1A: $Wo_{10–38}En_{0.4–46}Fs_{31–85}$; 12003,312_C: $Wo_{9.4–28}En_{2.7–30}Fs_{55–76}$). Although the distribution of pyroxene compositions within the type 2 samples is similar, those in 12003,308_2A are slightly more Fe-rich than those in 12003,308_4A, 12003,308_8A, and the 12003,310 samples (Figs. 5b, 6b, and 7b). Pyroxene in the type 3 samples and two of the type 4 samples (12003,308_3A and 12003,316_C) is more equilibrated than that in the other 12003 samples and is clearly separated into low-Ca ($Wo_{3.7–22}En_{51–66}Fs_{24–37}$) and high-Ca phases ($Wo_{27–41}En_{41–53}Fs_{15–23}$; Figs. 5d and 5e). The low-Ca pigeonite is more abundant than the high-Ca augite in all of the samples (Table 2).

Trivalent pyroxene REE concentrations in the 12003 samples vary between 0.06 to 120 × CI abundances (Fig. 8). The 12003 pyroxene grains typically have significantly higher concentrations of heavy REE than light REE, although the CI-normalized REE patterns become flatter toward the rims of the more compositionally zoned grains (La_{cn}/Lu_{cn} = 0.01–0.59). The high- and low-Ca pyroxene phases in the type 3 samples (12003,308_5A and 12003,308_7A) can also be distinguished by their REE concentrations, with the high-Ca phases having higher concentrations (up to 24 × CI values) than the low-Ca phases (up to 10 × CI abundances; Fig. 8e). This is not the case for the type 4 samples (12003,308_3A and 12003,316_C), however, in which the low- and high-Ca pyroxene REE concentrations are indistinguishable (Fig. 8f).

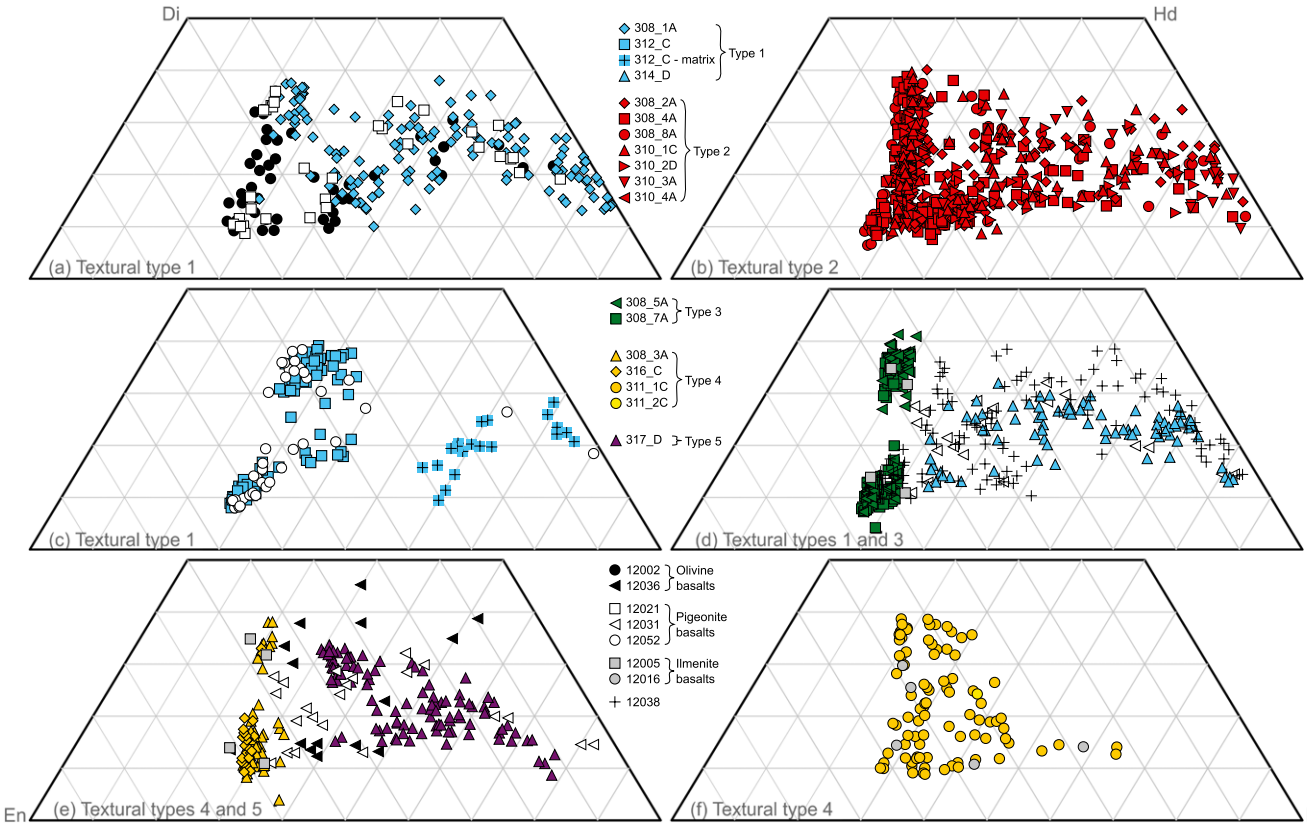

Fig. 5. Compositions of pyroxene phases within the 12003 chips. The 12003 pyroxene compositions are compared with those within other Apollo 12 samples (Bence et al. 1970; Boyd and Smith 1971; Brett et al. 1971; Keil et al. 1971; Grove et al. 1973; Dungan and Brown 1977; Beaty et al. 1979; Shearer et al. 1989). Di = diopside; Hd = hedenbergite; En = enstatite; Fs = ferrosilite.

Olivine

As with the pyroxene grains, the type 1 and 2 olivine phenocrysts are compositionally zoned (Table 4; Fig. 3b). Most of the type 2 olivine phenocrysts have compositions between $Fo_{39–74}$. A wider range of olivine compositions is noted within 12003,308_2A ($Fo_{3–73}$), which contains several small (approximately 10–50 μm) fayalite grains adjacent to the most evolved pyroxene rims. The olivines in type 1 sample, 12003,312_C, have less forsteritic core compositions ($Fo_{41–64}$) than those in the type 2 samples. By contrast, the compositionally equilibrated nature of the phases in the coarser grained type 3 samples (Figs. 5d, 6d, and 7d) is also apparent in the less zoned olivine compositions ($Fo_{61–68}$, respectively; Fig. 3b).

Minor Phases

The 12003 silica phases typically have SiO_2 between 96 and 98 wt%. The most abundant minor elements in the silica phases are Al, Ti, and Fe (Al_2O_3 = 0.4–0.8 wt%; TiO_2 = 0.2–0.5 wt%; FeO = 0.1–0.6 wt%). Relative to those in the other 12003 samples, the type 3 and 4 ilmenite grains have higher concentrations of MgO (1.7–6.4 wt%).

The spinel phases in 12003,312_C and the type 2 samples have mostly chromite compositions ($2Ti_{10–14}Al_{24–29}Cr_{59–66}$; 2Ti = atomic 2Ti/[2Ti+Al+Cr] × 100; Al = atomic Al/[2Ti+Al+Cr] × 100; Cr = atomic Cr/[2Ti+Al+Cr] × 100; Table 4). However, many of the larger crystals and glomerophyric clusters have ulvöspinel rims ($2Ti_{37–86}Al_{6–18}Cr_{8–45}$). Where the spinel grains are partially enclosed in or adjacent to mafic phenocrysts, the ulvöspinel rims occur around the edges that are not in contact with the phenocryst but are adjacent to the surrounding groundmass material (Figs. 2b and 2d). Some smaller chromite grains in the type 2 samples are entirely enclosed in olivine phenocrysts. The more coarsely grained type 3 and 4 lithologies also exhibit a wide range of spinel compositions ($2Ti_{19–80}Al_{7–32}Cr_{13–55}$). However, individual grains are typically more internally homogeneous, with the exception of patches of ilmenite exsolution, and follow a different trend in compositional evolution (Fig. 9a). By comparison, the spinel grains in 12003,314_D have a relatively narrow range of ulvöspinel compositions ($2Ti_{89–92}Al_{4–5}Cr_{4–7}$).

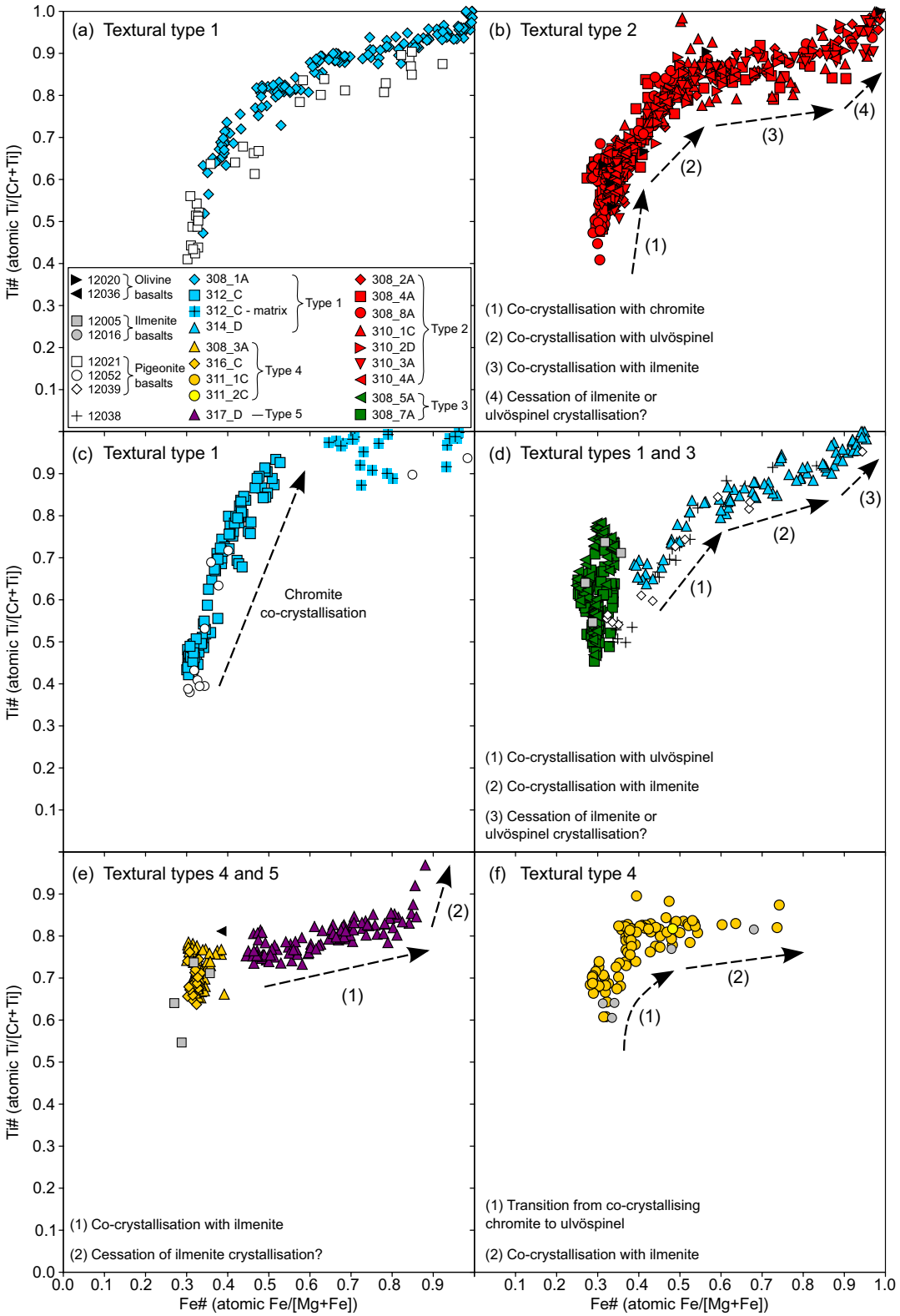

Fig. 6. Fe# (atomic Fe/[Mg+Fe] versus Ti# (atomic Ti/[Ti+Cr]) for pyroxene phases within samples 12003,308 1-10A. Compositions are compared with those reported for pyroxene in other Apollo 12 samples (Bence et al. 1970; Boyd and Smith 1971; Brett et al. 1971; Keil et al. 1971; Grove et al. 1973; Dungan and Brown 1977; Beaty et al. 1979; Shearer et al. 1989).

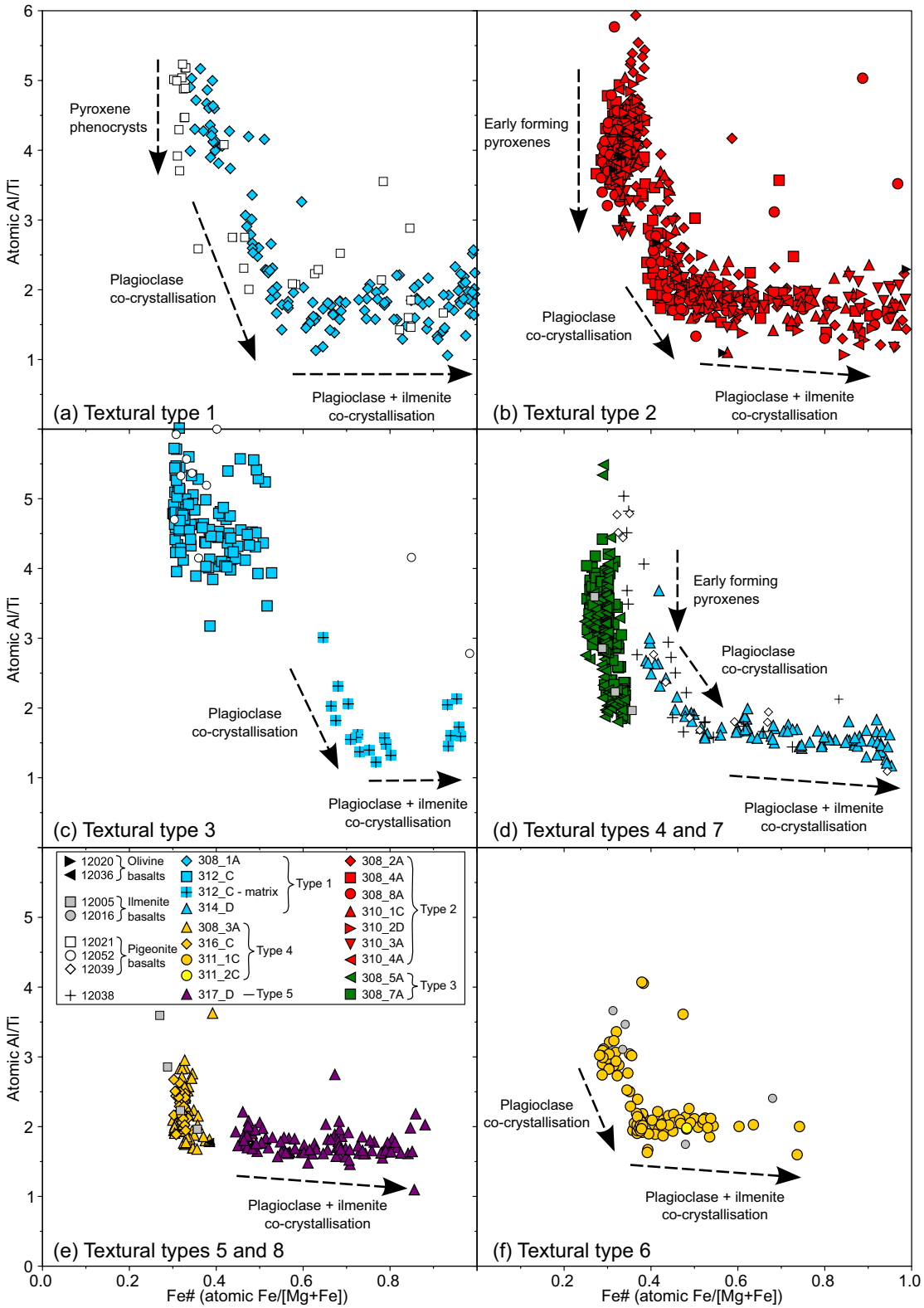

Fig. 7. Atomic Al/Ti versus Fe# (atomic Fe/[Mg+Fe]) for pyroxene phases within the 12003,308 samples. Compositions are compared with those reported for pyroxene in other Apollo 12 samples (Bence et al. 1970; Boyd and Smith 1971; Brett et al. 1971; Keil et al. 1971; Grove et al. 1973; Dungan and Brown 1977; Beaty et al. 1979; Shearer et al. 1989).

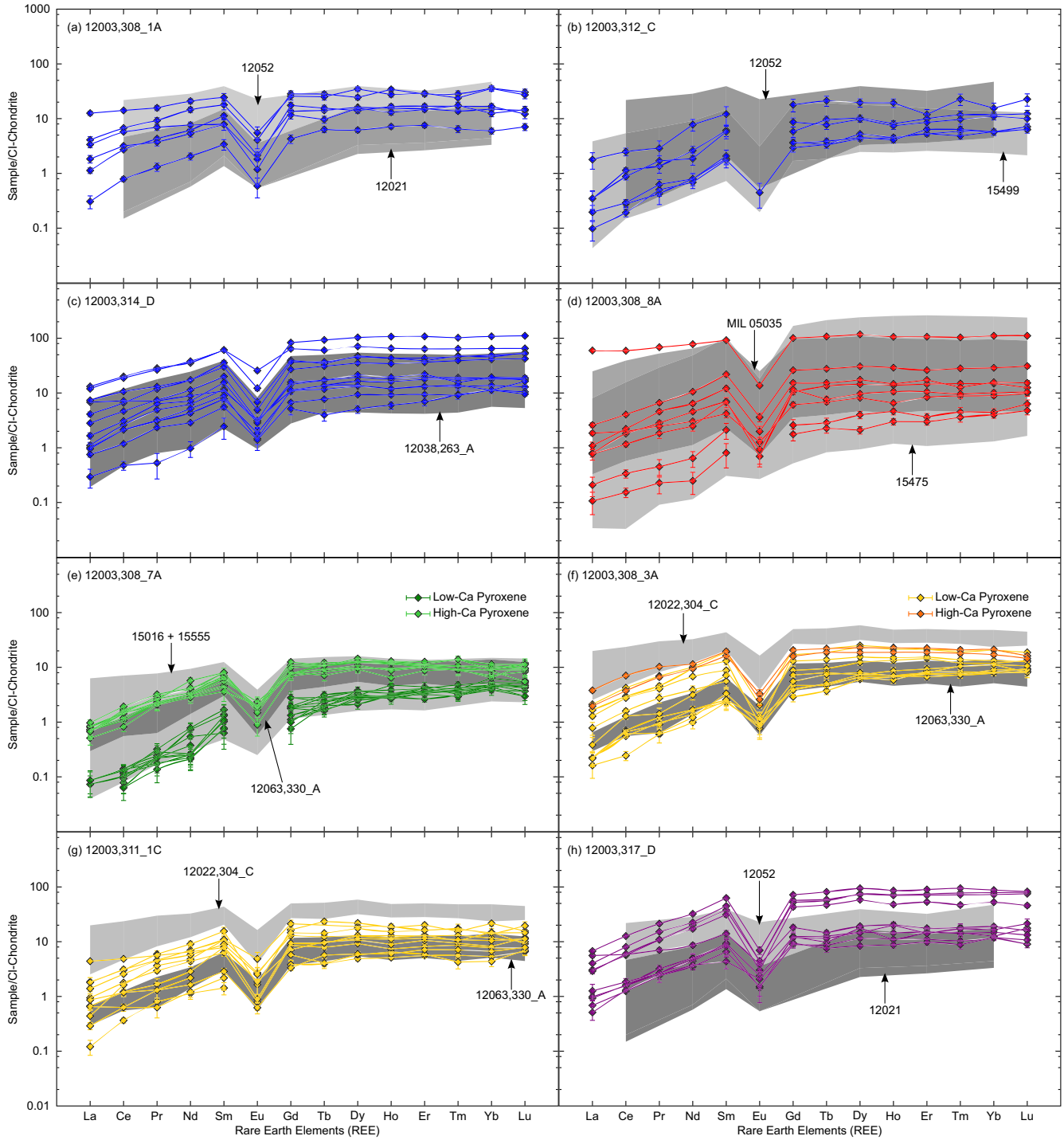

Fig. 8. Chondrite normalized (CI values of Anders and Grevesse 1989) REE patterns for pyroxene within 12003,308_1A; 12003,312_C; 12003,314_D; 12003,308_8A; 12003,308_7A; 12003,308_3A; 12003,311_1C; and 12003,317_D. Error bars represent 1σ errors. 12003 data have been compared with those obtained from: the pigeonite basalts 12021 and 12052 (Shearer et al. 1989); the ilmenite basalts 12022,304 and 12063,330; the feldspathic basalt 12038,263; the Apollo 15 low-Ti olivine-normative (15016 and 15555) and quartz-normative (15475 and 15499) basalts (Schnare et al. 2008); and the lunar meteorite MIL 05035 (Joy et al. 2008).

Accessory Phases

The 12003 sulfide grains exhibit typical lunar troilite compositions (S = 33–39 wt%; Fe = 60–66 wt%). A majority of the 12003 metal grains have FeNi compositions (Fe = 86–98 wt%; Ni = 1.8–13 wt%; Co = 1.0–2.3 wt%). However, a single more pure Fe

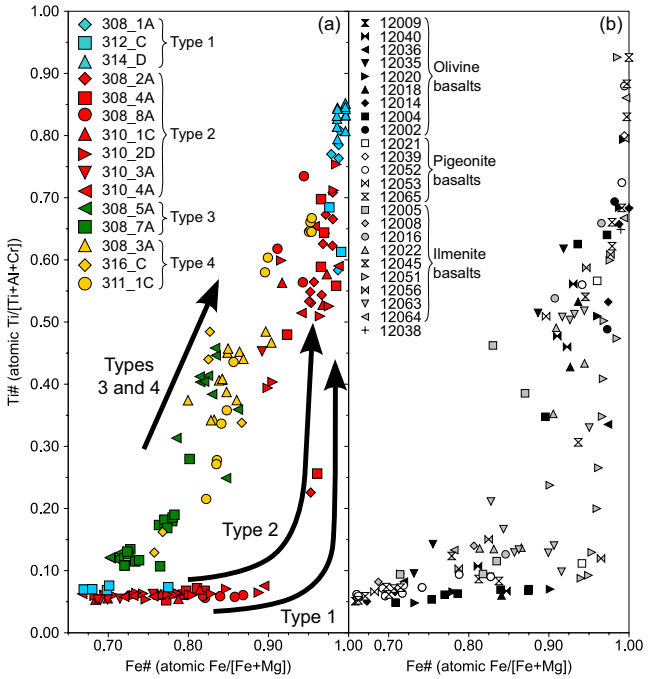

Fig. 9. Ti# (atomic Ti/[Ti+Al+Cr]) versus Fe# (atomic Fe/[Fe+Mg]) of spinel phases within the 12003 chips. 12003 spinel compositions (a) are compared with those reported in other Apollo 12 samples (b) (Gibb et al. 1970; Haggerty and Meyer 1970; Brett et al. 1971; Brown et al. 1971; Cameron 1971; Champness et al. 1971; El Goresy et al. 1971; Keil et al. 1971; Kushiro et al. 1971; Reid 1971; Simpson and Bowie 1971; Taylor et al. 1971; Weill et al. 1971; Dungan and Brown 1977).

metal grain (Fe = 100 wt%; Ni = 0.5 wt%; Co = 0.5 wt%) was identified in one of the type 2 samples (12003,310_3A), and the metal grains in 12003,314_D and 12003,317_D all contain between 98.5 and 99.5 wt% Fe and 1.0–1.2 wt% Co.

Where EMP WDS analyses were successfully made, a majority of the 12003 phosphate phases were determined to be apatite (P_2O_5 = 39–42 wt%; CaO = 53 wt%), with the exception of those in the type 3 samples (12003,308_5A and 12003,308_7A), which were identified as merrillite (P_2O_5 = 45 wt%; CaO = 46 wt%).

DISCUSSION

Evaluation of Bulk Sample Results

As referred to in the introduction, the representativeness of modal mineralogy and bulk chemistry measurements for small sample sizes is questionable. In their review of bulk analyses of Apollo 15 basalts, Ryder and Schuraytz (2001) determined that analyses of masses <1 g were inadequate to properly characterize such samples. Given that all of the 12003 samples analyzed in this study had masses <50 mg prior to mounting in epoxy and, furthermore, that their bulk compositions were determined on the basis of single cross section areas of these masses, we are extremely reluctant to overinterpret these values. The problem is clearly demonstrated with the samples 12003,311_1C and 12003,311_2C, which are known to originate from the same parent rock, yet have significantly different bulk TiO_2 values (2.5 and 0.98 wt%; Table 3) primarily due to different modal abundances of ilmenite (2 and <1%). Nevertheless, for finer grained samples (e.g., 12003,308_1A and 12003,312_C), the bulk chemistries and modal mineralogies can potentially provide useful information to be evaluated in conjunction with mineral chemistries.

Parent Melt Compositions

The Mg# of the parent melt ($Melt_{Mg\#}$) for a given basalt can be predicted from the Fo# of liquidus olivine phases ($Oliv_{Fo}$), assuming that these were in equilibrium with the melt when they formed. To do this, the following equation is used

$$Melt_{Mg\#} = 1/([1/Oliv_{Fo} - 1]/K_d + 1) \quad (1)$$

(Roedder and Emslie 1970; Niu et al. 2002) where K_d is the distribution coefficient describing the exchange of Fe and Mg between olivine and a coexisting basaltic melt (determined to be 0.33 for low pressure low-Ti lunar melts; Grove and Vaniman 1978; Longhi et al. 1978). By taking the most forsteritic olivine compositions in each of the 12003 chips as an estimate of $Oliv_{Fo}$, the $Melt_{Mg\#}$ for each chip has been calculated (Table 5).

It is also possible to predict $Oliv_{Fo}$ from $Melt_{Mg\#}$ by rearranging Equation (1) such that

$$Oliv_{Fo} = 1/(K_d \times [1/Melt_{Mg\#} - 1] + 1) \quad (2)$$

(Joy et al. 2008). If the bulk composition of a given basaltic sample is representative of the parent melt from which it crystallized, then the bulk Mg# $\approx$ $Melt_{Mg\#}$. This comparison is made for each sample in Table 5.

The predicted $Melt_{Mg\#}$ and $Oliv_{Fo}$ values for 12003,312_C and the type 2 samples are in reasonable agreement with the measured bulk Mg# and olivine compositions. This indicates that the bulk compositions of these chips are broadly representative of their parent melts. There is a significant discrepancy between the measured and predicted values for the type 3 and 4 samples. This may be due to unrepresentative sampling of the parent rock or compositional equilibration within the olivine modifying the initial phase compositions.

Table 5. Calculation of parent melt Mg# ($Melt_{Mg\#}$; atomic Mg/[Mg+Fe] × 100) and liquidus olivine Fo# ($Oliv_{Fo}$; atomic Mg/[Mg+Fe] × 100). For textural types of which there are multiple samples, an average of the samples has been calculated as well as a 1σ standard deviation.

		$Oliv_{Fo}$		$Melt_{Mg\#}$	
Textural type	Sample	Measured	Predicted	Measured[a]	Predicted
Type 1	12003,312_C	64.3	67.8	41.0	37.3
Type 2	12003,308_2A	73.1	76.0	51.1	47.3
	12003,308_4A	70.5	81.5	59.2	44.1
	12003,308_8A	74.4	82.5	60.9	49.0
	12003,310_1C	73.0	74.7	49.4	47.2
	12003,310_2D	71.7	79.1	55.6	45.6
	12003,310_3A	71.4	72.0	46.0	45.1
	12003,310_4A	72.5	78.4	54.5	46.5
	Average	72.4	77.8	53.8	46.4
	St. Dev.	±1.3		±5.3	
Type 3	12003,308_5A	68.1	85.9	66.9	41.4
	12003,308_7A	68.2	86.6	68.1	41.5
	(average)	68.2	86.3	67.5	41.4
	St. Dev.	±0.1		±0.8	
Type 4	12003,308_3A	72.7	80.9	58.3	46.8
	12003,316_C	66.3	82.0	60.1	39.3
	12003,311_1C	63.0	78.2	54.2	36.0
	12003,311_2C	60.6	79.4	56.0	33.7
	(average)	65.6	80.1	57.2	38.9
	St. Dev.	±5.2		±2.6	

[a]Bulk sample Mg# are use here as a proxy for the measured $Melt_{Mg\#}$.

It is also possible to calculate the REE composition of the basaltic melts from trace element mineral compositions. Several problems are known to exist with such calculations and have been described more fully elsewhere (e.g., Treiman 1996). The most significant problems are the lack of suitable partition coefficients for different phase compositions and crystallization conditions, and the equilibration of phases leading to the modification in their initial liquidus compositions. In addition to this, the extent of compositional zoning in many of the 12003 phases and relatively coarse laser spot size (55 μm) made it hard to ensure that the areas analyzed were homogeneous and representative of the most primitive core compositions.

Melt compositions were calculated from plagioclase analyses using the coefficients compiled by Snyder et al. (1992). The issue of suitable pyroxene partition coefficients was addressed using the method of Sun and Liang (2012, 2013) to calculate coefficients based on the compositions of individual pyroxene phases (see Appendices S4 and S5).

A majority of the 12003 plagioclase parent melts have trivalent REE concentrations of between approximately 10–300 × CI abundances (Fig. 10). The type 1, 2, 4, and 5 pyroxene parent melts have trivalent REE concentrations of between approximately 10–1000 × CI abundances. The type 3 pyroxene parent melt compositions are less varied with trivalent REE concentrations of approximately 3–70 × CI abundances (Fig. 10e).

The wide range of REE concentrations in the type 1, 2, and 5 pyroxene phases may be evidence of fractional crystallization (e.g., Fig. 8d). A similar effect might be also expected to result from the changing partition coefficients as the pyroxene compositions evolve. However, despite the variation in the calculated partition coefficients (see Appendix S4), the parent melts of these samples show a similarly wide range of REE concentrations (Fig. 10d), as would be expected from fractional crystallization of the melts. Contrary to the relatively narrow range of REE concentrations measured in the type 4 pyroxenes, the ranges of calculated parent melt compositions for these samples are as wide as those for the type 1, 2, and 5 samples and may, therefore, indicate fractional crystallization of the type 4 samples as well (Figs. 10f and 10g). The more narrow range of REE concentrations in the type 3 parent melts, on the other hand, indicates either a lower degree of fractionation during crystallization of these samples or subsolidus equilibration (Fig. 10e).

The similarity in REE concentrations between the low- and high-Ca pyroxenes in the type 4 samples (12003,308_3A and 12003,316_C) may imply the

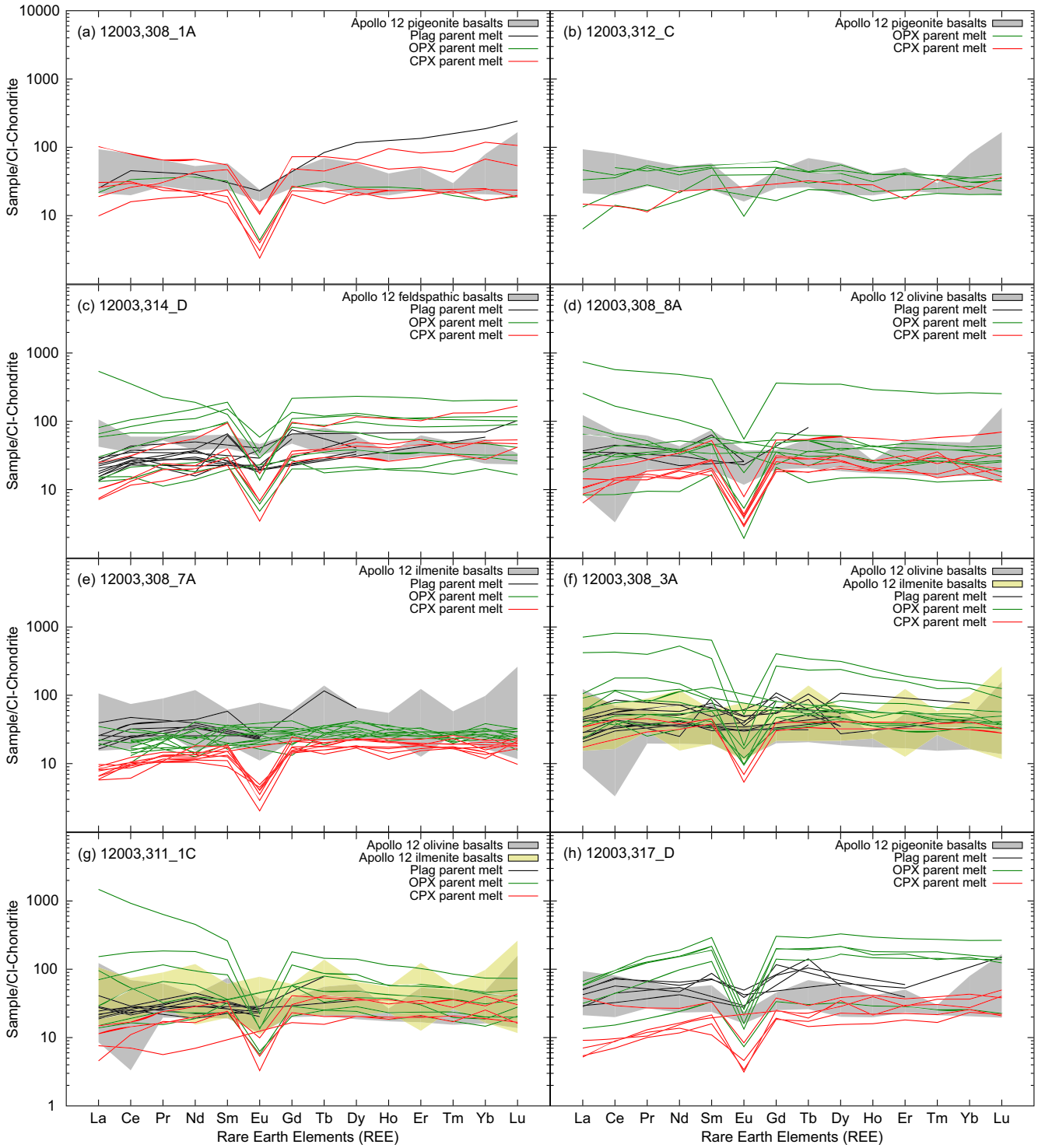

Fig. 10. Results of equilibrium parent melt reconstructions. The different lines represent the chondrite normalized (Anders and Grevesse 1989) REE compositions calculated for pyroxene and plagioclase phases in each of the samples. The pyroxene partition coefficients were calculated using the method outlined by Sun and Liang (2012, 2013). This method calculates separate orthopyroxene and clinopyroxene coefficients for phases with $Wo_{<25}$ or $Wo_{>25}$ (Wo = atomic Ca/[Fe+Mg+Ca] × 100). The pyroxene melt composition lines have been colored (see online version of manuscript for full-color figures) to discriminate between those calculated from orthopyroxene and clinopyroxene coefficients. The parent melt compositions have been compared with bulk compositions reported for the Apollo 12 pigeonite, feldspathic, olivine, and ilmenite basalts (see Clive Neal's mare basalt database and references therein).

Table 6. Summary of the inferred crystallization sequences for the 12003 chips.

	Crystallization sequence
Type 1 (12003,308_1A)	chromite phenocrysts → pyroxene phenocrysts → groundmass pyroxene → ulvöspinel → plagioclase → ilmenite
Type 1 (12003,312_C)	olivine phenocrysts + pyroxene phenocrysts → chromite phenocrysts → ulvöspinel → groundmass plagioclase → groundmass pyroxene → ilmenite
Type 1 (12003,314_D)	pyroxene → plagioclase → ulvöspinel → ilmenite
Type 2	olivine phenocrysts → chromite phenocrysts → pyroxene → ulvöspinel → plagioclase → ilmenite
Type 3	olivine + spinel → ?
Type 4	olivine + spinel → pyroxene → plagioclase → ilmenite
Type 5	pyroxene → plagioclase → pyroxene → ilmenite → silica

derivation of these phases from different magmas. Calculating the parent melt compositions for these samples does not provide conclusive evidence of this. The high-Ca pyroxene parent melts for both the type 3 and the type 4 samples tend to have lower REE concentrations than those of the low-Ca pyroxenes; however, the ranges of REE concentrations are not distinct but instead overlap (Fig. 10f). The light REE concentrations of the 12003,316_C high- and low-Ca pyroxene parent melts are distinct (Appendix S4), although this is likely an artifact of undersampling, especially given the wider range of parent melt REE compositions calculated for the 12003,308_3A low-Ca pyroxene phases.

Crystallization Histories

Crystallization sequences have been inferred from the textural relationships and major and minor element chemistries of the phases in the 12003 samples and are summarized in Table 6. The pyroxene, olivine, and chromite phenocrysts in the type 1 and 2 samples are interpreted as the first phases to crystallize. However, the order in which these formed is not always apparent on the basis of textural observations. In the type 2 samples, chromite grains are completely enclosed in olivine, but they are located toward the rims of the phenocrysts, indicating that olivine began to crystallize first and subsequently cocrystallized with chromite. The 12003,312_C (type 1) chromite grains are located on the edge of the larger mafic phenocrysts, but not completely enclosed, possibly suggesting slightly later crystallization of spinel. The location of the ulvöspinel rims of the type 1 and 2 chromite grains indicates that ulvöspinel began to crystallize after the olivine and (in the case of 12003,312_C) pyroxene phenocrysts. The plagioclase-pyroxene intergrowths in most of the type 1 and 2 samples are interpreted as evidence of the cocrystallization of the two phases (Figs. 2a–d) (Drever et al. 1973). The decreasing Al/Ti ratio in most of the type 1 and 2 pyroxenes also provides an indication of plagioclase cocrystallization beginning between pyroxene Fe# 0.30 and 0.40 (Figs. 7a and 7b). In the case of 12003,314_D, the association and intergrowth of these with the minor phases present is interpreted as evidence that both pyroxene and plagioclase were still crystallizing when silica, spinel, and ilmenite appeared on the liquidus. By contrast, the interstitial nature of the groundmass pyroxene in 12003,312_C suggests that it formed after the plagioclase laths (Fig. 2b).

Olivine and spinel are also interpreted to be the first phases to have crystallized in the coarser grained type 3 and 4 samples. Again, the location of spinel grains enclosed in, but toward the edge of the olivine crystals is interpreted as evidence that olivine began to crystallize first and then cocrystallized with spinel. The typically more anhedral interstitial nature of pyroxene and plagioclase in these samples indicates that they crystallized after the olivine and spinel (Figs. 2e–g). The pyroxene overgrowths in the 12003,311 olivine grains are also consistent with this interpretation.

With the exception of the type 3 and 4 samples, in which the phases are more compositionally homogeneous, the evolving major and minor element compositions of the mafic phases have also been used to determine crystallization sequences. The variation in Cr in the 12003 olivine phases typically begins to decrease rapidly as the olivine compositions evolve beyond $Fo_{\sim 65-70}$ (Fo# = atomic Mg/[Mg+Fe] × 100; Figs. 11a–c) and then less rapidly beyond $Fo_{\sim 55}$. This is particularly clear in the type 2 samples, and is interpreted as partitioning of Cr into cocrystallizing chromite and until the cocrystallizing spinel phase changes from chromite to ulvöspinel.

The effect of cocrystallizing spinel is also visible in the Ti# (atomic Ti/[Cr+Ti]) of the type 1 and 2 pyroxene phases (Fig. 6). This increases rapidly between Fe# approximately 0.30 and 0.40 (atomic Fe/[Mg+Fe]) as Cr is partitioned into cocrystallizing chromite, and then less rapidly beyond this point (Fig. 6). This indicates the partitioning of Ti into another phase, or increasing Cr in the pyroxene, most likely due to the crystallization of ulvöspinel. As the pyroxenes evolve beyond Fe# approximately 0.45–0.55, the Ti# increases

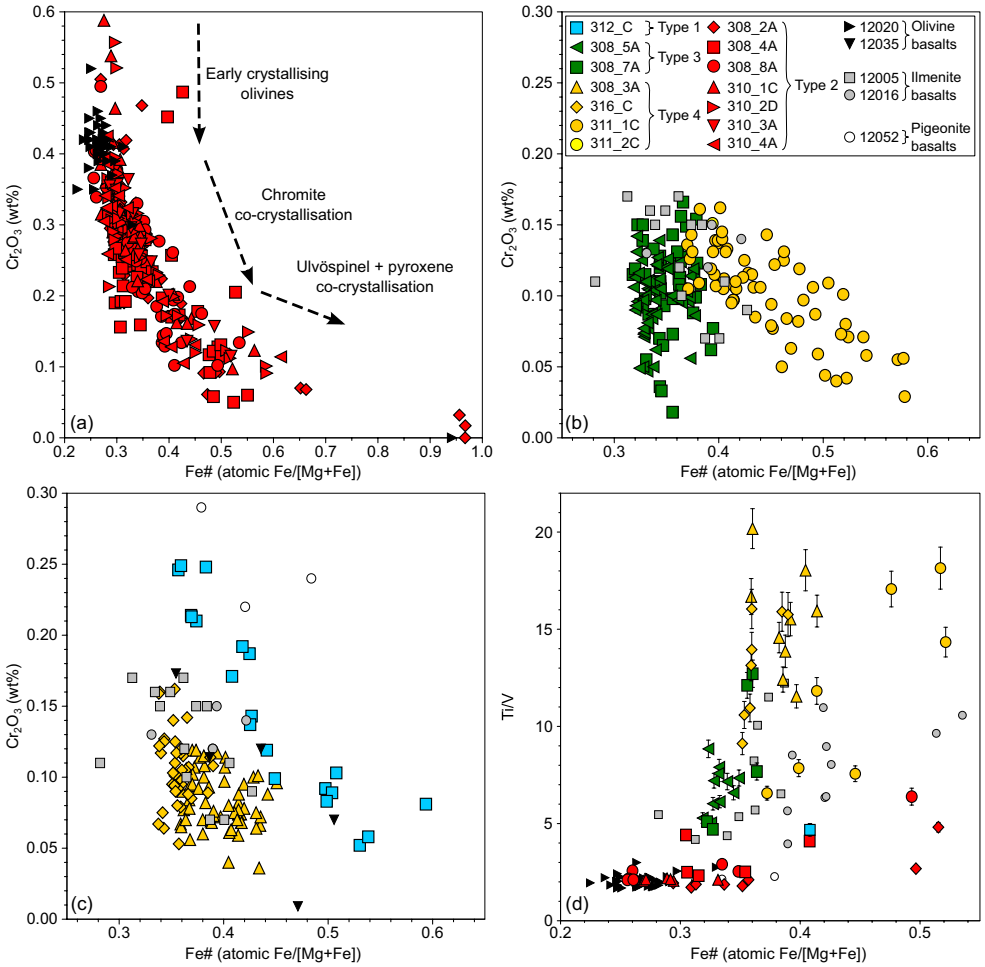

Fig. 11. (a–c) Cr_2O_3 wt% and (d) Ti/V versus Fe# (atomic Fe/[Fe+Mg]) in olivine phases within the 12003 samples. Note the reduced scales in (b and c) to account for the more limited compositional variations of the 12003 type 1, 3, and 4 olivine phases. Data are compared with those for olivine in other Apollo 12 basalts (Bence et al. 1970; Kushiro et al. 1971; Butler 1972; Dungan and Brown 1977; Fagan et al. 2013). Error bars represent 1σ errors.

even less rapidly, indicating further partitioning of Ti into another cocrystallizing phase, most likely ilmenite. The appearance of ilmenite on the liquidus at pyroxene Fe# approximately 0.40–0.55 is supported by the trend in pyroxene Al/Ti ratios (Fig. 7). Although similar trends are observed for the 12003,312_C pyroxenes, they tend to occur at later stages, with chromite cocrystallization occurring until the pyroxene compositions reach Fe# approximately 0.50, and crystallization of ilmenite not beginning until Fe# approximately 0.70. However, there is no clear indication in the type 5 pyroxene mineral chemistry that pyroxene cocrystallized with plagioclase, or began to crystallize prior to plagioclase or ilmenite.

The calculated parent melt REE abundances of the 12003 samples provide further information regarding crystallization histories. In the case of the type 1 and 2 samples, the plagioclase and pyroxene parent melts have overlapping ranges of REE abundances; however, the range of pyroxene parent melts in each sample begins at lower REE concentrations than those of the plagioclase parent melts. This is consistent with the pyroxene in these samples beginning to crystallize first and subsequently cocrystallizing with plagioclase. The lower REE abundances in the type 3 and 4 samples of the high-Ca pyroxene melts, compared with those for the low-Ca pyroxenes, indicate that the high-Ca phases began to crystallize first. In the type 3 samples, the range of REE concentrations in the plagioclase parent melts is higher than those in the high-Ca pyroxene melts, but overlaps with those in the low-Ca pyroxene melts. This is interpreted as evidence that the plagioclase began crystallizing after the high-Ca pyroxenes and was cocrystallizing with the low-Ca phases. This is not the case in the type 4 samples, where the plagioclase parent melt REE

abundances overlap with both the low- and high-Ca pyroxene parent melts.

For the type 5 sample, the plagioclase parent melts have REE abundances that lie mostly within a gap in the ranges of pyroxene melts. This may be suggestive of two distinct phases of pyroxene crystallization between which was a period of plagioclase crystallization. This is consistent with the texture of the sample, in which plagioclase is commonly enclosed by pyroxene. Furthermore, the most Fe-rich pyroxenes are commonly in interstitial areas in the plagioclase and surrounding the resorbed plagioclase grain boundaries (Fig. 2h).

Comparison with Other Apollo 12 Basalts

With two exceptions, the 12003 samples have low-Ti bulk compositions (Table 3) consistent with other Apollo 12 basaltic compositions. Samples 12003,311_2C and 12003,316_C have very low-Ti compositions (i.e., where bulk TiO_2 <1 wt%; Neal and Taylor 1992); however, the coarse grain sizes of these samples may result in bulk measurements, which are unrepresentative of the parental rocks. This is particularly noticeable in the case of 12003,311_2C (TiO_2 = 0.98 wt%), which almost certainly originated from the same parent chip as 12003,311_1C (TiO_2 = 2.48 wt%). Similarly, despite having an apparent very low bulk Ti composition (TiO_2 = 0.91 wt%), the Fe# and Ti# of the 12003,316_C pyroxene are more similar to those of low-Ti and high-Ti mare basalts (Fig. 6e) (Nielsen and Drake 1978; Arai et al. 1996; Robinson et al. 2012).

Although bulk Mg# values have been calculated for the 12003 samples (Table 3), it has not been possible to perform bulk trace element analyses that would provide a measure of their Rb/Sr ratios. The type 2, 3, and 4 samples all have Mg# ≥46 and, thus, fall within the range of either olivine or ilmenite basalts according to the Neal et al. (1994a, 1994b) scheme. The type 1 and 5 samples have lower Mg# (≤41) and are within the range of the feldspathic, pigeonite, or ilmenite basalts.

The bulk REE compositions of previously measured Apollo 12 samples are largely within the ranges of the calculated parent melt REE abundances for the 12003 samples. Unfortunately, the degree to which the bulk compositions from different basaltic suites overlap makes it very difficult to use this assign any of the 12003 samples to a particular suite.

Type 1

The type 1 samples 12003,308_1A and 12003,314_D lack olivine, and so are not likely to be members of the Apollo 12 olivine basalt suite. The lowest modal proportion of olivine reported in an olivine basalt is 5.7% (12072; Neal et al. 1994a). Similarities can be seen between these samples and the feldspathic, ilmenite, and pigeonite basaltic suites. The lack of olivine, plagioclase-rich nature, and correspondingly high concentrations of Al_2O_3 of the samples (Tables 2 and 3), makes them comparable to the feldspathic basalt 12038 (Neal et al. 1994a).

The 12003,308_1A sample has the highest bulk Ti-content of the 12003 samples (TiO_2 = 4.8 wt%), attributable to its relatively high ilmenite content (3.7% by mode). While a majority of the Apollo 12 ilmenite basalts are reported to have similar and relatively higher TiO_2 contents (James and Wright 1972; Rhodes et al. 1977; Neal et al. 1994b), the absence of olivine and the large amounts of silica in 12003,308_1A are less common features of the ilmenite basalt suite. However, several of the ilmenite basalts do have similar modal mineralogies to 12003,308_1A (e.g., 12047, 12061, 12062, and 12064; Klein et al. 1971; McGee et al. 1977; Dungan and Brown 1977; Neal et al. 1994a). The high modal abundance of silica in 12003,308_1A (6%) is also unusual for the Apollo 12 ilmenite basalts (James and Wright 1972; Neal et al. 1994a).

Low modal abundances of olivine and high abundances of silica are more common in the pigeonite basalts (e.g., samples 12007, 12021, 12031, 12039, 12043, and 12065; McGee et al. 1977; Baldridge et al. 1979; Neal et al. 1994a). Most of these basalts tend to be coarser grained than 12003,308_1A. The pigeonite basalt 12021 bears the closest textural resemblance to the type 1 sample. For example, 12003,308_1A has both the intrafasciculate and the radiate textures of 12021 described by Drever et al. (1972, 1973), which they suggest are the result of rapid cooling. Major and minor element compositional zoning of pyroxene in the type 1 sample is consistent with that observed in 12021 (Boyd and Smith 1971; Weill et al. 1971) (Fig. 5a). REE concentrations of pyroxenes in the type 1 sample are also consistent with those in the pigeonite basalt 12052, but have a larger range than those in 12021 (Shearer et al. 1989) (Fig. 8a). Plagioclase and spinel compositions reported for 12021 are also broadly similar with those of the type 1 sample (Figs. 3a and 9) (Weill et al. 1971; Crawford 1973).

Although a crystallization sequence has not been deduced for 12021, the crystallization sequences presented by Baldridge et al. (1979) for various pigeonite basalts are consistent with that inferred for 12003,308_1A from the pyroxene chemistries (chromite → pyroxene → ulvöspinel → plagioclase → ilmenite). Therefore, the sample is provisionally interpreted to be a small fragment of the same lava flows that sourced the Apollo 12 pigeonite basalts.

Several other porphyritic pigeonite basalts exist with similar textures to 12003,312_C (e.g., samples 12019,

12052, 12053, 12055). The modal mineralogy and bulk composition of 12003,312_C are also in good agreement with those reported for Apollo 12 pigeonite basalts, including the porphyritic samples 12019, 12052, and 12053 (Tables 2 and 3) (Papike et al. 1976; Papike and Vaniman 1978; Baldridge et al. 1979; Neal et al. 1994a).

The pyroxene compositions in the 12003,312_C phenocrysts are consistent with those reported for 12052 by Bence et al. (1970, 1971) and Shearer et al. (1989) (Figs. 5c and 8b). The 12003,312_C pyroxene REE compositions are also very similar to those measured in phenocrysts of low-Ti olivine- and quartz-normative Apollo 15 basalts (Fig. 8b) (Schnare et al. 2008). These include the quartz-normative basalt 15499, which has a similar porphyritic texture to 12003,312_C. The range of major element olivine compositions in 12003,312_C ($Fo_{41–64}$) is wider than that reported in 12052 ($Fo_{52–67}$; Figs. 3b and 11c) (Bence et al. 1970; Fagan et al. 2013), although only four 12052 olivine analyses are available for comparison. The single LA-ICP-MS analysis of olivine in 12003,312_C also indicates low concentrations of Ni and Co similar to those in 12052, although the Ti/V ratio of the 12003,312_C olivine is higher than those in the four available 12052 olivine analyses (Fagan et al. 2013). Spinel compositions were reported for 12052 by Gibb et al. (1970) and Haggerty and Meyer (1970). These are in good agreement with those measured in 12003,312_C (Fig. 9). Based on these observations, 12003,312_C is classified as a pigeonite basalt.

Sample 12003,314_D is texturally similar to the pigeonite basalts 12007, 12031, and 12039 and the feldspathic basalt 12038. The modal abundance of ilmenite in 12003,314_D is lower than that in 12038 and most pigeonite basalts. As such, the bulk TiO_2 concentration of 12003,314_D is also lower than that reported for either 12038 or any pigeonite basalts.

The major and minor element concentrations in the 12003,314_D pyroxene are comparable to those reported for 12038 (Keil et al. 1971; Beaty et al. 1979) and the pigeonite basalts 12021 and 12039 (Figs. 5d, 6d, and 7d) (Weill et al. 1971; Beaty et al. 1979; Shearer et al. 1989). It is noticeable that the most primitive (i.e., Mg-rich) 12003,314_D pyroxene phases are less Mg rich than those in 12038, and the most evolved 12003,314_D pyroxene are more Fe enriched. Pyroxene and plagioclase trace element data obtained from 12038,263, are also in good agreement from those of 12003,314_D (Figs. 4a and 8c). However, the most evolved 12003,314_D pyroxene phases also have higher REE than those in 12038,263. Both Simpson and Bowie (1971) and Keil et al. (1971) report the presence of ulvöspinel in 12038. As in 12003,314_D, this is described as containing exsolved ilmenite (Simpson and Bowie 1971). The Fe# and Cr# of the 12038 and 12003,314_D ulvöspinel are very similar; however, those in 12003,314_D have higher Ti#s (Fig. 9).

On balance, we interpret 12003,314_D as most likely being a slightly more evolved feldspathic basalt than 12038. If this interpretation is correct, it almost certainly crystallized from a separate lava flow to any of the other 12003 samples and would be notable as being one of the few currently recognized feldspathic basalts in the Apollo 12 sample collection (Neal et al. 1994a, 1994b). Neal et al. (1994a) speculated that 12038 may represent an exotic sample introduced to the Apollo 12 site by impact mixing or, alternatively, that feldspathic basalt flows were poorly sampled by the Apollo 12 mission. Since then, Korotev et al. (2011) have identified two small (19 and 36 mg) basaltic fragments as potential feldspathic basalts. Identification of further feldspathic basalts collected at different locations to 12038 would strengthen the case for feldspathic basalt flows being local to the Apollo 12 site. Weighted-average ages for each of the basaltic suites indicate that all three of the major suites were formed between approximately 3.18 and 3.20 Ga (Snyder et al. 1997). A slightly older average age (3.28 Ga) is reported for the feldspathic basalt 12038. If this is the case, and the feldspathic basalt flow underlies those of the other three suites, then the scarcity of feldspathic basalt samples could be due to a lack of craters large enough to excavate this material (Fig. 12).

Type 2

The 12003 type 2 samples have modal mineralogies, which are similar to those of the Apollo 12 olivine and ilmenite basalts (Grove et al. 1973; Neal et al. 1994a). The samples have lower bulk concentrations of TiO_2 and higher Mg# than most ilmenite basalts and are more similar to the bulk compositions of Apollo 12 olivine basalts (Neal et al. 1994a, 1994b). Texturally, the type 2 samples resemble the medium-grained porphyritic olivine basalt 12002. Grove et al. (1973) describe 12002 as containing phenocrysts of olivine and pyroxene, ilmenite laths, and "complexly zoned spinel with chromite cores overgrown by rims of chromian ulvöspinel." These features are observed in all of the type 2 samples. Many of the type 2 plagioclase crystals exhibit an intrafasciculate texture, which is also observed in 12002 (Drever et al. 1972; Grove et al. 1973).

Major and minor element compositions of pyroxene and olivine within the type 2 samples are consistent with those of 12002 and other olivine basalts (Figs. 3b, 5a, and 5b) (Grove et al. 1973). The wide range of type 2 pyroxene REE compositions (0.11–118 × CI values) exceeds those in the ilmenite (12022 and 12063—0.40–67.5 × CI values), pigeonite (0.15–47.2 × CI values;

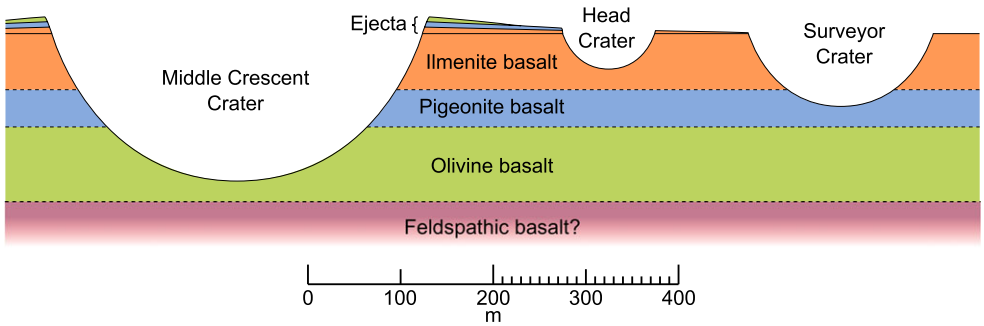

Fig. 12. Simplified theoretical cross section of the Apollo 12 site, indicating stratigraphic sequence as inferred by Rhodes et al. (1977) and the estimated excavation depths of the three largest craters at the landing site. Scale is approximate with a 2× vertical exaggeration applied. Note the lack of craters large enough to excavate the feldspathic basalt unit.

Shearer et al. 1989), and feldspathic (12038—0.19–56.8 × CI values) basalts for which trace data are available. However, the lunar meteorite MIL 05035 (0.33–110 × CI values; Joy et al. 2008) and the low-Ti Apollo 15 quartz-normative basalt 15475 (0.03–262 × CI values; Schnare et al. 2008) contain similarly wide ranges of pyroxene compositions resulting from fractional crystallization (Fig. 8d).

Several analyses of more evolved olivine ($Fo_{<60}$) in three of the type 2 samples have higher Ti/V ratios than previously observed in Apollo 12 olivine basalts (Fagan et al. 2013), although mineral trace element data are currently only available for three basalts from the olivine suite and do not include analyses of similarly evolved olivine (Fig. 11d). Ni and Co concentrations in the type 2 olivine phases are generally higher than those in the other 12003 samples and most similar to those in olivine basalts (Fig. 13). Once again, exceptions to this are the most evolved olivine phases in one of the samples (12003,308_8A), which have lower concentrations of Ni and Co than those reported in other olivine basalts. Type 2 basalt olivine Ni concentrations appear to decrease throughout crystallization (Fig. 13a), as has been observed in other low-Ti lunar basalts (Karner et al. 2003), and so lower Ni concentrations in the type 2 12003 olivine may again be due to a lack of previous trace element analyses of evolved olivine. Conversely, Karner et al. (2003) observed incompatible behavior of Co in lunar olivine, making the lower Co concentrations in two of the more evolved 12003,308_8A olivine phases harder to explain, when compared with those in other type 2 samples such as 12003,308_2A and 12003,308_4A.

The spinel compositions in the type 2 samples are also comparable to those described in 12002 and a number of other variolitic and subophitic basalts within the Apollo 12 olivine and ilmenite suites (e.g., 12014, 12063, and 12065; Reid 1971; Taylor et al. 1971; El Goresy et al. 1971) (Fig. 9).

The type 2 olivine and pyroxene chemistries have been used to infer the following crystallization sequence: olivine → chromite → pyroxene → ulvöspinel → plagioclase → ilmenite. This is in good agreement with the sequence of Apollo 12 basalt 12002 that Walker et al. (1976) derived from phase-equilibria and cooling rate studies. As such, the type 2 samples are inferred to be fragments of the same lava flows that sourced the Apollo 12 olivine basalts.

Type 3

The 12003 type 3 samples have modal mineralogies unlike any of the main Apollo 12 basaltic groups (Table 2; Papike and Vaniman 1978). Several olivine vitrophyre samples (e.g., 12008, 12009, 12015) do have similarly low modal abundances of plagioclase, but also contain significantly more olivine and less pyroxene than the 12003 type 3 samples (Brett et al. 1971; Papike et al. 1976; Baldridge et al. 1979; Neal et al. 1994a). The textures of these olivine vitrophyres, with their fine-grained matrices and skeletal, dendritic, and euhedral olivine phenocrysts, are quite unlike the more coarsely grained type 3 samples with their rounded olivine grains (James and Wright 1972; Rhodes et al. 1977; Baldridge et al. 1979) (Figs 2e). The ilmenite basalt 12005 is also reported to have low abundances of plagioclase and, although it too contains more olivine and less pyroxene than the type 3 samples, the cumulate texture described by Rhodes et al. (1977) and Dungan and Brown (1977) is more similar to that of 12003,308_5A and 12003,308_7A. 12005 has the highest Mg content of any previously studied Apollo 12 basalt (MgO = 19.97 wt%; Rhodes et al. 1977). This is very close to the values measured for 12003,308_5A (MgO = 19.9 wt%) and 12003,308_7A (MgO = 18.6 wt%; Table 3).

Apollo 12 sample 12005 also has a similar range of olivine and pyroxene compositions to the type 3 samples (Figs. 3b, 5d, 6d, and 7d) (Dungan and Brown 1977). For example, in addition to their unusually

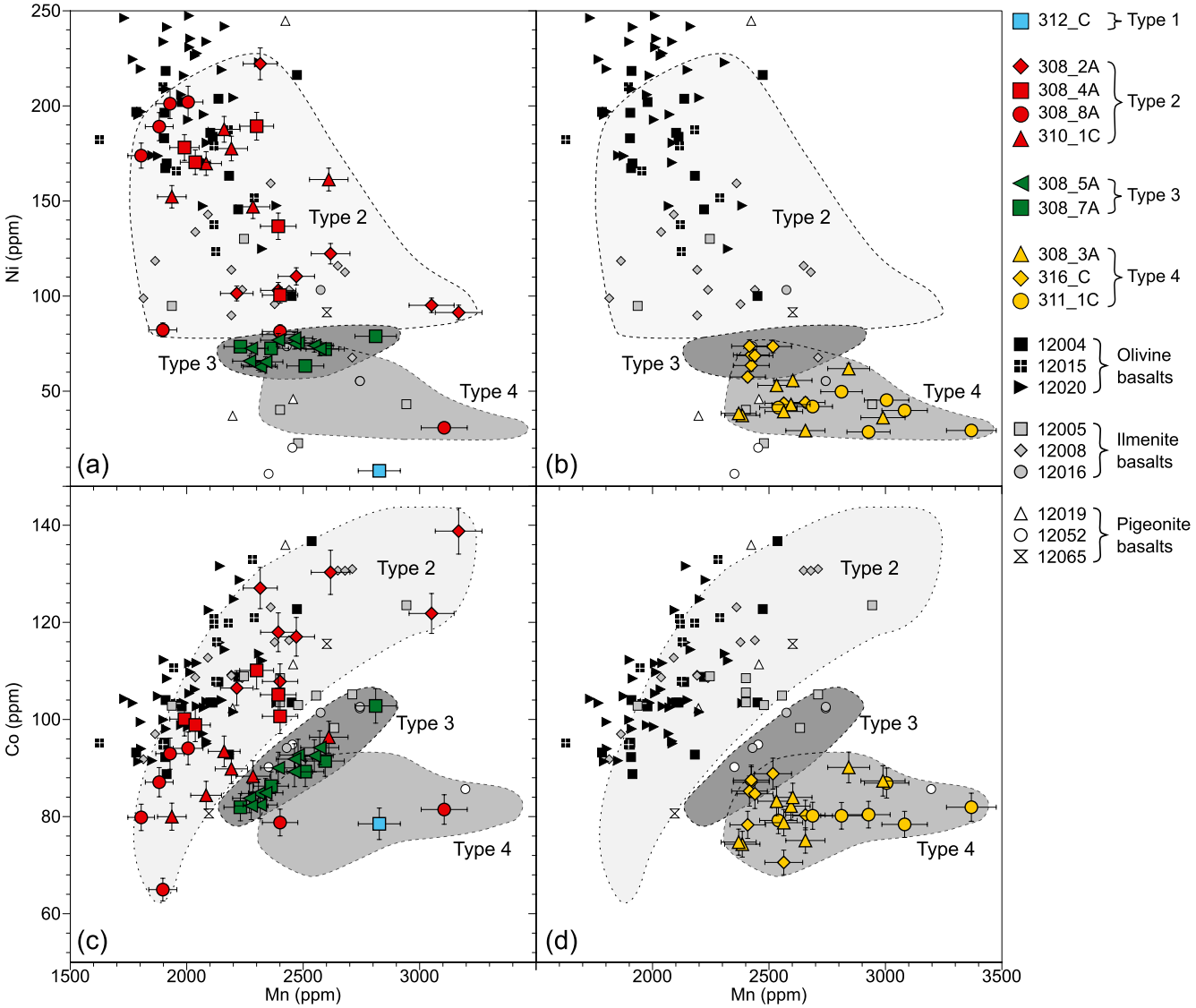

Fig. 13. (a, b) Ni and (c, d) Co versus Mn ppm concentrations in olivine phases within the 12003 samples. Mn behaves incompatibly in olivine and can, therefore, be used as an indicator of igneous fractionation (Karner et al. 2003). Data are compared with those for olivines in other Apollo 12 basalts (Fagan et al. 2013). Error bars represent 1σ errors.

narrow compositional range, many of the clinopyroxene phases within 12003,308_5A and 12003,308_7A are less Fe-rich than most clinopyroxene phases in the other 12003 samples or other Apollo 12 basalts (Figs. 5d, 6d, and 7d). The Ti/V ratios of the type 3 olivines are also consistent with those of other Apollo 12 ilmenite basalts and are in particularly good agreement with those of 12005 (Fig. 11d) (Fagan et al. 2013). Ni and Co concentrations of the type 3 olivines are lower than those in Apollo 12 olivine basalts with equivalent Mn concentrations, but are within the range of those in ilmenite basalts (Fig. 13). REE analyses of pyroxene in 12005 are not currently available; however, the REE concentrations in pyroxene phases of ilmenite basalt 12063,330 are in good agreement with those of the augite phases in the 12003 type 3 basaltic samples (Fig. 8e). The type 3 pigeonite phases have lower REE abundances (trivalent REE = 0.06–9.75 × CI values) than pyroxene in either of the pigeonite basalts analyzed by Shearer et al. (1989) (0.38–317 × CI values) or any of the three well-characterized samples analyzed in this study (12022 = 2.54–67.5 × CI values; 12038 = 0.19–56.8 × CI values; 12063 = 0.26–135 × CI values). In addition to this, the pyroxene parent melts calculated for the type 3 samples have REE abundances that are either at the low end or below the range of the bulk REE compositions previously reported in other Apollo 12 basalts (Fig. 10e). This suggests that the samples

represent more primitive basalts. The REE abundances of the type 3 pigeonite phases are more similar to pyroxene in the Apollo 15 low-Ti olivine-normative basalts 15016 and 15555 (Fig. 8e) (Schnare et al. 2008).

Dungan and Brown (1977) also report the compositions of spinel in 12005, which fall along a similar trend to the type 3 basalt spinel on a plot of Ti# against Fe# (Fig. 9). As with the type 3 basalt spinel, those in 12005 commonly exhibit ilmenite exsolution (Dungan and Brown 1977). The high-Mg content of the ilmenite in 12003,308_5A also correlates with the ilmenite analyses reported by Dungan and Brown (1977) for 12005. Dungan and Brown (1977) also report the compositions of metal grains in 12005 (Ni = approximately 6–18 wt%; Co approximately 2 wt%), which are comparable to those in 12003,308_5A (Ni = 1.8–12 wt%; Co = 1.8–2.4 wt%). Based on these observations, the type 3 samples are interpreted to be fragments of primitive ilmenite basalts.

Type 4

The 12003 type 4 samples are also unlike most Apollo 12 basaltic samples. The modal mineralogy of 12003,308_3A is similar to those reported by Brett et al. (1971) and Papike et al. (1976) for the olivine basalt 12035. Samples 12035 and 12003,308_3A also have (1) similar bulk compositions (Table 3; Compston et al. 1971); (2) similar olivine compositions (Figs. 3b and 11c) (Butler 1972); and (3) similar spinel compositions (Fig. 9) (Reid 1971). Reid (1971) described this sample as a gabbro (see also James and Wright 1972) with a cumulate texture and interpreted the spinel compositions and textural characteristics as being consistent with materials that crystallized early and accumulated toward the bottom of a lava flow, while the other finer grained olivine basalts represented the near-surface layers of the flow. Similar pyroxene, olivine, and spinel compositions are also observed between 12003,308_3A, 12003,316_C, and the ilmenite basalt 12005 (Figs. 5e, 6e, 7e, 9, and 11c) (Dungan and Brown 1977). Sample 12005 is one of the only Apollo 12 samples identified as containing similarly equilibrated pigeonite and augite phases (Dungan and Brown 1977).

The textures of the 12003,311_1C and 12003,311_2C samples reflect those in the equigranular ilmenite basalt 12016 (Fig. 2g) (Dungan and Brown 1977). The modal mineralogies of the two 12003,311 samples (Table 2) are also comparable to those reported for 12016 (Dungan and Brown 1977; Neal et al. 1994a). The major and minor element concentrations of the 12003,311 pyroxene, olivine, and spinel phases are also in very good agreement with those from the ilmenite basalt 12016 (Figs. 3b, 5f, 6f, 7f, and 9). Despite these similarities, the 12003,311 samples have less ilmenite, lower bulk concentrations of TiO_2, and higher bulk Mg# than any of the ilmenite basalts (Neal et al. 1994a). Given the comparatively coarse-grained textures and small sizes of these samples, this can almost certainly be attributed to unrepresentative sampling of the parent rock.

The type 4 basalt olivine phases have lower Co concentrations than those in any of the previously studied olivine or ilmenite basalts, and a majority of pigeonite basalts (Fig. 13d). The ratios of Ti/V for many of the type 4 olivine phases are also higher than those in any previously studied Apollo 12 basalt (Fig. 11d) (Fagan et al. 2013). Limited olivine trace element data are currently available for comparison, and it could be argued that these features may be due to differing crystallization conditions and variations in cocrystallizing phases such as spinel resulting in low concentrations of V and higher Ti (e.g., Karner et al. 2003; De Hoog et al. 2010). However, similarly coarse-grained samples (including 12005) with similar inventories of ilmenite and spinel were analyzed by Fagan et al. (2013). When compared with bulk compositions determined for olivine and ilmenite basalts, the parent melt compositions calculated for the type 4 samples have relatively high REE abundances (Figs. 10f and 10g). This suggests that these samples cannot simply be explained as more primitive members of these basaltic suites. When combined with the samples' unusual modal mineralogy, these observations may indicate that the 12003 type 4 samples represent slowly cooled basalts from the base of a previously unrecognized low-Ti lava flow (Day and Taylor 2007), or perhaps a subsurface magma chamber.

Type 5

The texture of the type 5 sample 12003,317_D is similar to the more granular texture described by Beaty et al. (1979) in the pigeonite basalt 12031. The abundances of minor phases within the two samples are very similar; however, 12031 has more plagioclase and less pyroxene than 12003,317_D. It contains more Fe (Mg# = 33.3) than 12031 (Mg# = 43.1; Rhodes et al. 1977), but the bulk composition of 12003,317_D is, in general, similar to that of the pigeonite basalts.

Sample 12031 is reported to have a wide range of plagioclase compositions ($An_{48–98}$; Beaty et al. 1979). The range of plagioclase compositions measured within 12003,317_D ($An_{77–94}$), therefore, is well within this range (Fig. 3a). The most primitive pyroxene compositions of 12031 are significantly more magnesian than those in 12003,317_D (Fig. 5e). As such, if the two samples do originate from similar sources, then 12003,317_D may represent the product of a later stage of crystallization than 12031. This is also consistent with the difference in bulk Mg# between the two

samples. A more evolved parent melt for 12003,317_D may also explain why the most REE-rich pyroxenes in the sample exceed those of other pigeonite basalts (Fig. 8h) (Shearer et al. 1989).

SUMMARY

A total of 17 separate basaltic chips have been studied from the 12003 soil. Analysis of these samples indicates that all three of the major Apollo 12 basaltic suites (olivine, ilmenite, and pigeonite basalts) are represented in the soil collected at a single location near the Lunar Module landing site.

One sample (12003,314) has been identified as a possible addition to the feldspathic suite, currently represented by only one other confirmed sample (12038). 12003,314_D has a subophitic-intergranular texture, similar to that of 12038 and several pigeonite basalts (e.g., 12007, 12031, and 12039). It has a higher modal abundance of plagioclase (55%) and bulk Al_2O_3 (16.5 wt%) than any other Apollo 12 basalt. The mineral chemistries of 12003,314_D are in good agreement with those reported in both 12038 and the pigeonite basalts. However, given the sample's bulk-rock characteristics and textural similarity to 12038, it is interpreted as most likely being a feldspathic basalt. If correct, this has important implications for the diversity of Apollo 12 basalts as it would strengthen the argument that the feldspathic basalts are not exotic to the Apollo 12 site, as suggested by Neal et al. (1994a, 1994b), but represent a poorly sampled basaltic flow, possibly underlying the landing site (Fig. 12).

Three samples (type 4 samples 12003,308_3A, 12003,316 and 12003,311) have been identified in the 12003 soil, which may represent a previously unrecognized basaltic suite. The 12003,308_3A and 12003,316 samples have high abundances of olivine and low abundances of pyroxene relative to other Apollo 12 basalts, although these modal mineralogies are to be viewed with caution due to the comparatively coarse grain size (up to approximately 0.8 mm) of the samples when compared with the overall surface areas studied (<4.4 mm^2). These have comparatively compositionally equilibrated minerals and olivine with higher Ti/V ratios and lower concentrations of Co than are currently reported for any other Apollo 12 basalts.

The range of textures and mineral chemistries in the 12003 samples indicates a variety of crystallization conditions. The compositional zoning identified in the phases of a majority of the samples is consistent with fractional crystallization resulting, for example, in the concentration of REE toward the rims of phases. The type 3 samples are interpreted as having formed through slower equilibrium crystallization toward the base of thick lava flows (Reid 1971; Day and Taylor 2007) or prior to eruption.

Based on the geochemical diversity presented in this study, it is proposed that between 5–6 individual basaltic flows would be required to generate the 12003 chips analyzed. This would include the olivine, pigeonite, ilmenite, and (probably) feldspathic basalt flows previously identified, in addition to the basal flows/shallow level magma chambers from which the type 4 samples are inferred to have crystallized. However, interpretations of the differences between the samples' mineral chemistry, and the significance of these differences, are limited by the current availability of published trace element mineral chemistry data for other Apollo 12 basalts. It is hoped that future studies will provide new data sets, allowing for more incisive comparisons to be made.

Acknowledgments—The authors thank Drs. Andy Beard and Andrew Carter at Birkbeck for their assistance using the JEOL SEM and LA-ICP-MS systems. This manuscript was greatly improved by the thorough reviews of Clive Neal and Katharine Robinson. We are also grateful to Karl Cronberger (University Notre Dame) for input in the calculation of pyroxene partition coefficients. This research has made use of NASA's Astrophysics Data System and Clive Neal's Mare Basalt Database.

Editorial Handling—Dr. Christian Koeberl

REFERENCES

Albee A. L., Quick J. E., and Chodos A. A. 1977. Source and magnitude of errors in "broad-beam analysis" (DBA) with the electron probe. Proceedings, 8th Lunar Science Conference. pp. 7–9.

Anders E. and Grevesse N. 1989. Abundances of the elements —Meteoritic and solar. *Geochimica et Cosmochimica Acta* 53:197–214.

Anderson A. T. Jr. and Smith J. V. 1971. Nature, occurrence, and exotic origin of "gray mottled" (Luny Rock) basalts in Apollo 12 soils and breccias. Proceedings, 2nd Lunar Science Conference. pp. 431–438.

Arai T., Warren P. H., and Takeda H. 1996. Four lunar mare meteorites: Crystallization trends of pyroxenes and spinels. *Meteoritics & Planetary Science* 31:877–892.

Baldridge W. S., Beaty D. W., Hill S. M. R., and Albee A. L. 1979. The petrology of the Apollo 12 pigeonite basalt suite. Proceedings, 10th Lunar and Planetary Science Conference. pp. 141–179.

Beaty D. W., Hill S. M. R., Albee A. L., and Baldridge W. S. 1979. Apollo 12 feldspathic basalts 12031, 12038 and 12072—Petrology, comparison and interpretations. Proceedings, 10th Lunar and Planetary Science Conference. pp. 115–139.

Bence A. E., Papike J. J., and Prewitt C. T. 1970. Apollo 12 clinopyroxenes: Chemical trends. *Earth and Planetary Science Letters* 8:393–399.

Bence A. E., Papike J. J., and Lindsley D. H. 1971. Crystallization histories of clinopyroxenes in two porphyritic rocks from Oceanus Procellarum. Proceedings, 2nd Lunar Science Conference. pp. 559–574.

Boyd F. R. and Smith D. 1971. Compositional zoning in pyroxenes from lunar rock 12021, Oceanus Procellarum. *Journal of Petrology* 12:439–464.

Brett R., Butler P. Jr., Meyer C. Jr., Reid A. M., Takeda H., and Williams R. 1971. Apollo 12 igneous rocks 12004, 12008, 12009, and 12022: A mineralogical and petrological study. Proceedings, 2nd Lunar Science Conference. pp. 301–317.

Brown G. M., Emeleus C. H., Holland J. G., Peckett A., and Phillips R. 1971. Picrite basalts, ferrobasalts, feldspathic norites, and rhyolites in a strongly fractionated lunar crust. Proceedings, 2nd Lunar Science Conference. pp. 583–600.

Butler P. Jr. 1972. Compositional characteristics of olivines from Apollo 12 samples. *Geochimica et Cosmochimica Acta* 36:773–785.

Cameron E. N. 1971. Opaque minerals in certain lunar rocks from Apollo 12. Proceedings, 2nd Lunar Science Conference. pp. 193–206.

Champness P. E., Dunham A. C., Gibb F. G. F., Giles H. N., MacKenzie W. S., Stumpfl E. F., and Zussman J. 1971. Mineralogy and petrology of some Apollo 12 lunar samples. Proceedings, 2nd Lunar Science Conference. pp. 359–376.

Compston W., Berry H., Vernon M. J., Chappell B. W., and Kaye M. J. 1971. Rubidium-strontium chronology and chemistry of lunar material from the Ocean of Storms. Proceedings, 2nd Lunar Science Conference. pp. 1471–1485.

Crawford I. A., Fagents S. A., and Joy K. H. 2007. Full Moon exploration: Valuable (non-polar) lunar science facilitated by a return to the Moon. *Astronomy and Geophysics* 48:3.18–3.21.

Crawford M. L. 1973. Crystallization of plagioclase in mare basalts. Proceedings, 4th Lunar Science Conference. pp. 705–717.

Day J. M. D. and Taylor L. A. 2007. On the structure of mare basalt lava flows from textural analysis of the LaPaz Icefield and Northwest Africa 032 lunar meteorites. *Meteoritics & Planetary Science* 42:3–17.

Deer W. A., Howie R. A., and Zussman J. 1966. *An introduction to the rock-forming minerals*. London: Longman.

De Hoog J. C., Gall L., and Cornell D. H. 2010. Trace-element geochemistry of mantle olivine and application to mantle petrogenesis and geothermobarometry. *Chemical Geology* 270:196–215.

Dowty E., Prinz M., and Keil K. 1973. Composition, mineralogy, and petrology of 28 mare basalts from Apollo 15 rake samples. Proceedings, 4th Lunar Science Conference. pp. 423–444.

Drever H. I., Johnston R., Butler P. Jr., and Gibb F. G. F. 1972. Some textures in Apollo 12 lunar igneous rocks and in terrestrial analogs. Proceedings, 3rd Lunar Science Conference. pp. 171–184.

Drever H. I., Johnston R., and Brebner G. 1973. Radiate texture in lunar igneous rocks and terrestrial analogs. Proceedings, 4th Lunar Science Conference. pp. 187–189.

Dungan M. A. and Brown R. W. 1977. The petrology of the Apollo 12 ilmenite basalt suite. Proceedings, 8th Lunar Science Conference. pp. 1339–1381.

El Goresy A., Ramdohr P., and Taylor L. A. 1971. The opaque minerals in the lunar rocks from Oceanus Procellarum. Proceedings, 2nd Lunar Science Conference. pp. 219–235.

Fagan A. L., Neal C. R., Simonetti A., Donohue P. H., and O'Sullivan K. M. 2013. Distinguishing between Apollo 14 impact melt and pristine mare basalt samples by geochemical and textural analyses of olivine. *Geochimica et Cosmochimica Acta* 106:429–445.

Gibb F. G. F., Stumpfl E. F., and Zussman J. 1970. Opaque minerals in an Apollo 12 rock. *Earth and Planetary Science Letters* 9:217–224.

Grove T. L. and Vaniman D. T. 1978. Experimental petrology of very low Ti (VLT) basalts. In *Mare Crisium: The view from Luna 24*, edited by Merrill R. B. and Papike J. J. New York: Pergamon Press. pp. 445–471.

Grove T. L., Walker D., Longhi J., Stolper E., and Hays J. F. 1973. Petrology of rock 12002 and origin of picritic basalts at Oceanus Procellarum. Proceedings, 4th Lunar Science Conference. pp. 995–1011.

Haggerty S. E. and Meyer H. O. A. 1970. Apollo 12: Opaque oxides. *Earth and Planetary Science Letters* 9:379–387.

Hiesinger H. and Head J. W. 2006. New views of lunar geoscience: An introduction and overview. In *New views of the Moon*, edited by Jolliff B. L., Wieczorek M. A., Shearer C. K., and Neal C. R. Washington, D.C.: Mineralogical Society of America. pp. 1–83.

Hiesinger H., Jaumann R., Neukum G., and Head J. W. 2000. Ages of mare basalts on the lunar nearside. *Journal of Geophysical Research* 105:29239–29276.

Hiesinger H., Head J. W., Wolf U., Jaumann R., and Neukum G. 2003. Ages and stratigraphy of mare basalts in Oceanus Procellarum, Mare Nubium, Mare Cognitum, and Mare Insularum. *Journal of Geophysical Research (Planets)* 108:5065.

Hiesinger H., Head J. W., Wolf U., Jaumann R., and Neukum G. 2010. Ages and stratigraphy of lunar mare basalts in Mare Frigoris and other nearside maria based on crater size-frequency distribution measurements. *Journal of Geophysical Research (Planets)* 115:E03003.

Hollister L. S., Trzcienski W. E. Jr., Hargraves R. B., and Kulick C. G. 1971. Petrogenetic significance of pyroxenes in two Apollo 12 samples. Proceedings, 2nd Lunar Science Conference. pp. 529–557.

James O. B. and Wright T. L. 1972. Apollo 11 and 12 mare basalts and gabbros: Classification, compositional variations, and possible petrogenetic relations. *Geological Society of America bulletin* 83:2357–2382.

Joy K. H., Crawford I. A., Anand M., Greenwood R. C., Franchi I. A., and Russell S. S. 2008. The petrology and geochemistry of Miller Range 05035: A new lunar gabbroic meteorite. *Geochimica et Cosmochimica Acta* 72:3822–3844.

Joy K. H., Crawford I. A., Russell S. S., and Kearsley A. T. 2010. Lunar meteorite regolith breccias: An in situ study of impact melt composition using LA-ICP-MS with implications for the composition of the lunar crust. *Meteoritics & Planetary Science* 45:917–946.

Joy K. H., Burgess R., Hinton R., Fernandes V. A., Crawford I. A., Kearsley A. T., and Irving A. J. 2011. Petrogenesis and chronology of lunar meteorite Northwest Africa 4472: A KREEPy regolith breccia from the Moon. *Geochimica et Cosmochimica Acta* 75:2420–2452.

Karner J., Papike J. J., and Shearer C. K. 2003. Olivine from planetary basalts: Chemical signatures that indicate

planetary parentage and those that record igneous setting and process. *American Mineralogist* 88:806–816.

Karner J., Papike J. J., and Shearer C. K. 2004. Plagioclase from planetary basalts: Chemical signatures that reflect planetary volatile budgets, oxygen fugacity, and styles of igneous differentiation. *American Mineralogist* 89:1101–1109.

Karner J., Papike J. J., and Shearer C. K. 2006. Comparative planetary mineralogy: Pyroxene major- and minor-element chemistry and partitioning of vanadium between pyroxene and melt in planetary basalts. *American Mineralogist* 91:1574–1582.

Keil K., Prinz M., and Bunch T. E. 1971. Mineralogy, petrology, and chemistry of some Apollo 12 samples. Proceedings, 2nd Lunar Science Conference. pp. 319–341.

Klein C. Jr., Drake J. C., and Frondel C. 1971. Mineralogical, petrological, and chemical features of four Apollo 12 lunar microgabbros. Proceedings, 2nd Lunar Science Conference. pp. 265–284.

Korotev R. L., Jolliff B. L., Zeigler R. A., Seddio S. M., and Haskin L. A. 2011. Apollo 12 revisited. *Geochimica et Cosmochimica Acta* 75:1540–1573.

Kushiro I., Nakamura Y., Kitayama K., and Akimoto S.-I. 1971. Petrology of some Apollo 12 crystalline rocks. Proceedings, 2nd Lunar Science Conference. pp. 481–495.

Li L. and Mustard J. F. 2005. On lateral mixing efficiency of lunar regolith. *Journal of Geophysical Research (Planets)* 110:11,002–11,018.

Longhi J. 1992a. Experimental petrology and petrogenesis of mare volcanics. *Geochimica et Cosmochimica Acta* 56:2235–2251.

Longhi J. 1992b. Origin of picritic green glass magmas by polybaric fractional fusion. Proceedings, 22nd Lunar and Planetary Science Conference. pp. 343–353.

Longhi J., Walker D., and Hays J. F. 1978. The distribution of Fe and Mg between olivine and lunar basaltic liquids. *Geochimica et Cosmochimica Acta* 42:1545–1558.

Lunar Sample Preliminary Examination Team (L.S.P.E.T.). 1970. Preliminary examination of lunar samples from Apollo 12. *Science* 167:1325–1339.

Marvin U. B. and Walker D. 1985. A transient heating event in the history of a highlands troctolite from Apollo 12 soil 12033. Proceedings, 15th Lunar and Planetary Science Conference. pp. 421–429.

McGee P. E., Warner J. L., and Simonds C. H. 1977. Introduction to the Apollo collections. Part 1: Lunar igneous rocks. NASA STI/Recon Technical Report N 77: 22034.

Morota T., Haruyama J., Ohtake M., Matsunaga T., Honda C., Yokota Y., Kimura J., Ogawa Y., Hirata N., Demura H., Iwasaki A., Sugihara T., Saiki K., Nakamura R., Kobayashi S., Ishihara Y., Takeda H., and Hiesinger H. 2011. Timing and characteristics of the latest mare eruption on the Moon. *Earth and Planetary Science Letters* 302:255–266.

Neal C. R. and Taylor L. A. 1992. Petrogenesis of mare basalts—A record of lunar volcanism. *Geochimica et Cosmochimica Acta* 56:2177–2211.

Neal C. R., Hacker M. D., Snyder G. A., Taylor L. A., Liu Y. G., and Schmitt R. A. 1994a. Basalt generation at the Apollo 12 Site, Part 1: New data, classification, and re-evaluation. *Meteoritics* 29:334–348.

Neal C. R., Hacker M. D., Taylor L. A., Schmitt R. A., and Liu Y.-G. 1994b. Basalt generation at the Apollo 12 site, part 2: Source heterogeneity, multiple melts, and crustal contamination. *Meteoritics* 29:349–361.

Newton R. C., Anderson A. T., and Smith J. V. 1971. Accumulation of olivine in rock 12040 and other basaltic fragments in the light of analysis and syntheses. Proceedings, 2nd Lunar Science Conference. pp. 575–582.

Nielsen R. L. and Drake M. J. 1978. The case for at least three mare basalt magmas at the Luna 24 landing site. In *Mare Crisium: The view from Luna 24*, edited by Merrill R. B. and Papike J. J. New York: Pergamon Press. pp. 419–428.

Niu Y., Gilmore T., Mackie S., Greig A., and Bach W. 2002. Mineral chemistry, whole-rock compositions, and petrogenesis of LEG 176 gabbros: Data and discussion. In *Proceedings of the Ocean Drilling Program, scientific results*, edited by Natland J. H., Dick H. J. B., Miller D. J. and Von Herzen R. P. Chapter 8, vol. 176. College Sation, Texas: Integrated Ocean Drilling Program. pp. 1–60.

Papike J. J. and Vaniman D. T. 1978. Luna 24 ferrobasalts and the mare basalt suite—Comparative chemistry, mineralogy, and petrology. In *Mare Crisium: The view from Luna 24*, edited by Merrill R. B. and Papike J. J. New York: Pergamon Press. pp. 371–401.

Papike J. J., Hodges F. N., Bence A. E., Cameron M., and Rhodes J. M. 1976. Mare basalts—Crystal chemistry, mineralogy, and petrology. *Reviews of Geophysics and Space Physics* 14:475–540.

Papike J. J., Taylor L., and Simon S. 1991. Lunar minerals. In *The lunar sourcebook*., edited by Heiken G., Vaniman D., and French B. M. Cambridge: Cambridge University Press. pp. 121–181.

Pearce N. J. G., Perkins W. T., Westgate J. A., Gorton M. P., Jackson S. E., Neal Clive R., and Chenery S. P. 1997. A compilation of new and published major and trace element data for NIST SRM 610 and NIST SRM 612 glass reference materials. *Geostandards and Geoanalytical Research* 21:115–144.

Quick J. E., Albee A. L., Ma M.-S., Murali A. V., and Schmitt R. A. 1977. Chemical compositions and possible immiscibility of two silicate melts in 12013. Proceedings, 8th Lunar Science Conference. pp. 2153–2189.

Rasband W.S. 1997–2013. *ImageJ*. Bethesda, Maryland: U.S. National Institutes of Health, http://imagej.nih.gov/ij/. Last accessed July, 2013.

Reid J. B. Jr. 1971. Apollo 12 spinels as petrogenetic indicators. *Earth and Planetary Science Letters* 10:351–356.

Rhodes J. M., Brannon J. C., Rodgers K. V., Blanchard D. P., and Dungan M. A. 1977. Chemistry of Apollo 12 mare basalts—Magma types and fractionation processes. Proceedings, 8th Lunar Science Conference. pp. 1305–1338.

Robinson K. L., Treiman A. H., and Joy K. H. 2012. Basaltic fragments in lunar feldspathic meteorites: Connecting sample analyses to remote sensing. *Meteoritics & Planetary Science* 47:387–399.

Roedder P. L. and Emslie R. F. 1970. Olivine-liquid equilibrium. *Contributions to Mineralogy and Petrology* 29:275–289.

Ryder G. and Schuraytz B. C. 2001. Chemical variation of the large Apollo 15 olivine-normative mare basalt rock samples. *Journal of Geophysical Research* 106:1435–1451.

Schnare D. W., Day J. M. D., Norman M. D., Liu Y., and Taylor L. A. 2008. A laser-ablation ICP-MS study of Apollo 15 low-titanium olivine-normative and quartz-normative mare basalts. *Geochimica et Cosmochimica Acta* 72:2556–2572.

Schneider C. A., Rasband W. S., and Eliceiri K. W. 2012. NIH Image to ImageJ: 25 years of image analysis. *Nature Methods* 9:671–675.

Shearer C. K., Papike J. J., Simon S. B., and Shimizu N. 1989. An ion microprobe study of the intra-crystalline behavior of REE and selected trace elements in pyroxene from mare basalts with different cooling and crystallization histories. *Geochimica et Cosmochimica Acta* 53:1041–1054.

Simpson P. R. and Bowie S. H. U. 1971. Opaque phases in Apollo 12 samples. Proceedings, 2nd Lunar Science Conference. pp. 207–218.

Snape J. F. 2012. Studies of the petrologic and geochemical diversity of the lunar regolith. PhD thesis, University College London, London, UK.

Snape J. F., Beaumont S., Burgess R., Crawford I. A., and Joy K. H. 2011a. An evaluation of techniques used in the age and petrologic analysis of Apollo 12 basalts (abstract #2011). 42nd Lunar and Planetary Science Conference. CD-ROM.

Snape J. F., Joy K. H., and Crawford I. A. 2011b. Characterization of multiple lithologies within the lunar feldspathic regolith breccia meteorite Northeast Africa 001. *Meteoritics & Planetary Science* 46:1288–1312.

Snyder G. A., Taylor L. A., and Neal C. R. 1992. A chemical model for generating the sources of mare basalts—Combined equilibrium and fractional crystallization of the lunar magmasphere. *Geochimica et Cosmochimica Acta* 56:3809–3823.

Snyder G. A., Neal C. R., Taylor L. A., and Halliday A. N. 1997. Anatexis of lunar cumulate mantle in time and space: Clues from trace-element, strontium, and neodymium isotopic chemistry of parental Apollo 12 basalts. *Geochimica et Cosmochimica Acta* 61:2731–2747.

Sun C. and Liang Y. 2012. Distribution of REE between clinopyroxene and basaltic melt along a mantle adiabat: Effects of major element composition, water, and temperature. *Contributions to Mineralogy and Petrology* 163:807–823.

Sun C., and Liang Y. 2013. Distribution of REE and HFSE between low-Ca pyroxene and lunar picritic melts around multiple saturation points. *Geochimica et Cosmochimica Acta* 119:340–358.

Taylor L. A., Kullerud G., and Bryan W. B. 1971. Opaque mineralogy and textural features of Apollo 12 samples and a comparison with Apollo 11 rocks. Proceedings, 2nd Lunar Science Conference. pp. 855–871.

Treiman A. H. 1996. The perils of partition: Difficulties in retrieving magma compositions from chemically equilibrated basaltic meteorites. *Geochimica et Cosmochimica Acta* 60:147–155.

U.S. Geological Survey. *Geochemical reference materials and certificates*. http://crustal.usgs.gov/geochemical_reference_standards/ (last accessed – 2013).

Van Achterberg E., Ryan C. G., Jackson S. E., and Griffin W. L. 2001. Data reduction software for LA-ICP-MS. *Mineralogical Association of Canada, Short Course Notes* 29:239–243.

Walker D., Kirkpatrick R. J., Longhi J., and Hays J. F. 1976. Crystallization history of lunar picritic basalt sample 12002—Phase-equilibria and cooling-rate studies. *Geological Society of America Bulletin* 87:646–656.

Warren P. H. 1997. The unequal host-phase density effect in electron probe defocused Beam analysis: An easily correctable problem (abstract #1497). 28th Lunar and Planetary Science Conference Abstracts. CD-ROM.

Weill D. F., Grieve R. A., McCallum I. S., and Bottinga Y. 1971. Mineralogy-petrology of lunar samples. Microprobe studies of samples 12021 and 12022; viscosity of melts of selected lunar compositions. Proceedings, 2nd Lunar Science Conference. pp. 413–430.

Wilson S. A. 1997. *The collection, preparation, and testing of USGS reference material BCR-2, Columbia River*. Geological Survey Open-File Report: Basalt. U.S. 98.

Zolensky M. E., Pieters C., Clark B., and Papike J. J. 2000. (Invited Review) Small is beautiful: The analysis of nanogram-sized astromaterials. *Meteoritics & Planetary Science* 35:9–29.

SUPPORTING INFORMATION

Additional supporting information may be found in the online version of this article:

Appendix S1: WDS data.

Appendix S2: LA-ICP-MS data.

Appendix S3: Backscattered electron images and false color element maps of the 12003 samples not included in the main figures.

Appendix S4: Additional material regarding the calculation of parent melt REE compositions for each of the 12003 samples. Including chondrite normalized plots of the measured pyroxene and plagioclase REE concentrations in each sample (accompanied by maps indicating the analysis locations) and reconstructed parent melt compositions. Also included are plots of the calculated pyroxene partition coefficients.

Appendix S5: Tabulated partition coefficients calculated for the pyroxene phases of each of the 12003 samples.